

**A SIMPLE APPROACH TO VISCOELASTIC MATERIAL SELECTION
FOR IMPACT ABSORPTION**

by

Stephen Makau Kimanzi

B.A.Sc. The University of British Columbia, 2016

A THESIS SUBMITTED IN PARTIAL FULFILLMENT OF
THE REQUIREMENTS FOR THE DEGREE OF

MASTER OF APPLIED SCIENCE

in

THE COLLEGE OF GRADUATE STUDIES

(Mechanical Engineering)

THE UNIVERSITY OF BRITISH COLUMBIA

(Okanagan)

January 2019

© Stephen Makau Kimanzi, 2019

The following individuals certify that they have read, and recommend to the College of Graduate Studies for acceptance, a thesis/dissertation entitled:

**A SIMPLE APPROACH TO VISCOELASTIC MATERIAL
SELECTION FOR IMPACT ABSORPTION**

submitted by Stephen Makau Kimanzi in partial fulfillment of the requirements of

the degree of MASTER OF APPLIED SCIENCE.

Dr. Rudolf Seethaler, Faculty of Applied Science

Supervisor

Dr. Hadi Mohammadi, Faculty of Applied Science

Supervisory Committee Member

Dr. Abbas Milani, Faculty of Applied Science

Supervisory Committee Member

Dr. Solomon Tesfamariam, Faculty of Applied Science

University Examiner

Abstract

Engineering materials are broadly classified as elastic or viscous but many materials exhibit a combination of both behaviors. This subgroup of materials is called viscoelastic because it combines the energy absorbing properties of elastic materials and the energy dissipation properties of viscous materials. This combination of properties makes them ideal for many applications including impact absorption. However, the complex and extensive mathematical nature of viscoelastic characterization and modeling has limited the majority of viscoelastic applications to tedious experimental work based on a trial and error. The problem with this approach is that experimental setups are not always available and are often time consuming when multiple material options are available. Therefore, this research takes on the mathematical modeling of viscoelastic materials for impact absorption to create reliable design curves that can readily predict viscoelastic material behavior based on a set of initial conditions.

By modeling the impact problem as a second order mass-spring-damper system, this work uses the Kelvin-Voigt viscoelastic model to relate experimentally measurable material parameters to those derived from the impact model. Use is made of the Ashby method to create an impact performance equation with acceleration as the performance metric. A Dynamic Mechanical Analyzer is used to obtain the material parameters for varying frequencies and design curves are generated using these parameters and the Ashby performance metric. Drop tower validation experiments are then conducted to compare the predicted acceleration values based on the impact model to actual impacts. The predicted-to-actual peak acceleration ratio approaches unity with lower peak drop tower strains. The results of this research show that viscoelastic mathematical modeling is not as complicated as once thought and that with a few assumptions, models can produce remarkably accurate results thereby cutting down on exhaustive experimental work.

Lay Summary

The purpose of this research is to develop a procedure for selecting materials whose behavior differs from commonly available engineering materials. These materials have properties that make them useful for impact absorption applications like shoes, running surfaces, cushioning materials, and helmets among others. The challenge with selecting these materials is that their behavior depends on multiple parameters such that creating performance equations requires extensive mathematical work. This has led to most applications being based on trial and error which increases both time and cost. The work presented in this research tackles the mathematical aspect of this analysis and creates readily applicable design curves for selecting the best material for impact absorption. Validation experiments conducted at the end of this analysis show that the quality of mathematical modeling done as well as the assumptions made do not significantly impact the quality of the results. Therefore, the work done here shows that it is possible to mathematically model and predict the response of these non-standard behaving materials without necessarily conducting extensive experiments which significantly improves the ability of designers to reduce cost of products designed for impact absorbing applications.

Preface

In order to develop solutions to the challenges that plague the development of better products, especially in material engineering, it is necessary to take on extensive computational tasks that have been previously avoided due to lack of computation power. However, the increased research and development for better performing materials, selecting optimal materials without exhausting resources through repeated experiments to determine their performance has become more challenging. With the availability of higher processing power capable of solving the complex mathematical expressions, there is an opportunity to create theoretical expressions capable of determining optimal materials and their performance with minimal experimental work. My goal is to create these expressions by solving these complicated mathematical equations and simplify them to fit day to day material selection applications. This will not only create an avenue for future research into modeling materials and predicting their behavior but will also show that such an endeavor is feasible with an impressive degree of success.

With tasks such as the one I have undertaken in this study, the support of family and friends is integral for success and I thank them for their unwavering support. I would also like to extend my gratitude to my thesis committee for their professional critique and guidance throughout my research work.

Table of Contents

Abstract	iii
Lay Summary	iv
Preface	v
Table of Contents	vi
List of Tables	x
List of Figures	xi
List of Symbols	xiii
List of Abbreviations	xiv
Acknowledgements	xv
Dedication.....	xvi
Chapter 1: Introduction	1
1.1 Application Definitions	2
1.1.1 Impact Absorption.....	2
1.2 Viscoelastic Materials Definitions.....	3
1.3 Thesis Organization	4
Chapter 2: Literature Review	5
2.1 Energy Dissipation in Mechanical Systems	6
2.1.1 Impact Absorption.....	7
2.2 Viscoelastic Materials	11
2.2.1 Maxwell-Wiechert Fluid Model	15
2.2.2 Kelvin-Voigt Solid Model.....	19
	vi

2.2.3	Standard Linear Solid	22
2.2.4	Viscoelastic Material Dynamic Behaviour.....	27
2.2.4.1	Mathematical Loss and Storage modulus.....	29
2.2.4.1.1	Maxwell-Wiechert Fluid.....	31
2.2.4.1.2	Kelvin-Voigt Solid.....	32
2.2.4.1.3	Standard Linear Solid.....	33
2.2.4.2	Experimental Loss & Storage Moduli.....	33
2.2.4.2.1	Maxwell Model.....	34
2.2.4.2.2	Kelvin Model.....	35
2.2.5	Modelling Viscoelastic Materials.....	35
2.3	Ashby Material Selection	36
2.3.1	Function	36
2.3.2	Constraints.....	37
2.3.3	Objective	37
2.3.4	Free Variable.....	38
Chapter 3: Design Equations		39
3.1	Impact Absorption.....	39
3.1.1	Equivalent Stiffness and Damping Coefficient	43
3.1.2	Impact Model Ashby Performance Equation	46
3.1.3	Impact Absorption Design Curves	50
Chapter 4: Instrumentation and Data Analysis		54
4.1	Dynamic Mechanical Analysis & Linear Viscoelasticity	54

4.2	Experimental Procedure.....	58
4.2.1	DMA Q800.....	59
4.2.2	Material Samples	60
4.2.3	DMA Instrument Calculations	61
4.3	Data Processing	62
4.4	Ashby Performance Ranking.....	64
4.5	Design Curves and Material Ranking.....	66
Chapter 5: Validation and Discussion		69
5.1	Validation Experiments.....	69
5.2	Discussion.....	73
Chapter 6: Conclusion		81
Bibliography		83
Appendices.....		87
Appendix A.....		87
A.1	Linear Viscoelastic Materials Constitutive Equation	87
A.2	Stress relaxation Modulus Fourier Transform.....	91
A.3	Experimental Loss and Storage Moduli	93
Appendix B.....		94
B.1	Damping Ratio change with Frequency	94
B.2	Predicted Peak Strain Calculation	94
B.3	Viscous Model Simulated Response	95
Appendix C.....		97

C.1	Data Tables	97
C.2	Sample Calculations	103

List of Tables

Table 2-1: Non-classical Material Behavior.....	12
Table 2-2: Non-classical Materials Rheological Models.....	13
Table 2-3: Equivalent SLS Model Rheological Operators	23
Table 3-1: Impact absorption problem definition	40
Table 4-1: Q800 Specifications [36]	59
Table 4-2: Experimental Sample Dimensions and Typical Specifications.....	61
Table 4-3: Material Property Summary	64
Table 5-1: Single Layer Material Performance, $ALm \cong 0.01$	74
Table 5-2: Two Layer Performance, $ALm \cong 0.005$	76
Table 5-3: Three Layer Performance, $ALm \cong 0.0033$	78
Table 5-4: Anelastic Material Behavior	80
Table C-1: Sorbothane Sample Raw Material Data	97
Table C-2: Neoprene Sample Raw Material Data.....	98
Table C-3: Rubber Sample Raw Material Data.....	100
Table C-4: Santoprene Sample Raw Material Data.....	101

List of Figures

Figure 2-1: Helmet Parts [33]	8
Figure 2-2: Standard Linear Solid Creep-Recovery Curve	14
Figure 2-3: Standard Linear Solid Stress Relaxation-Recovery Curve	14
Figure 2-4: Maxwell-Wiechert Fluid Model.....	15
Figure 2-5: Maxwell-Wiechert Stress relaxation (a) and Creep (b) responses	18
Figure 2-6: Kelvin-Voight Solid Model.....	19
Figure 2-8: Kelvin-Voigt Model Stress relaxation (a) and Creep (b) Responses	21
Figure 2-9: Standard Linear Solid using K-V (a) and M-W (b)	22
Figure 2-10: SLS Model Stress relaxation Behavior.....	26
Figure 2-11: SLS Model Creep Behavior.....	27
Figure 2-12: Dynamic Viscoelastic Response (© 1999 Roderic Lakes, by permission)	28
Figure 2-13: Viscoelastic Material Complex Modulus Argand Plane	30
Figure 3-1: Second order model for Impact Analysis	41
Figure 3-2: Viscous Model for Viscoelastic Materials.....	44
Figure 3-3: Argand Plane representation of Viscous Model	44

Figure 3-4: Impact Absorption Ashby Performance Curves	48
Figure 3-5: Sample Material Performance Design Curves	52
Figure 4-1: DMA Q800 (© Stephen Kimanzi).....	55
Figure 4-2: Typical DMA Configuration (© 1999 Kevin Menard, by permission)	55
Figure 4-3: DMA Sinusoidal Force-Displacement Plot (© 1999 Kevin Menard, by permission)	56
Figure 4-4: Linear Viscoelastic Range Behavior [36]	58
Figure 4-5: DMA Q800 Schematic for axial deformation mode [36].....	59
Figure 4-6: Superimposed Ashby Performance Curves for Material Selection.....	65
Figure 4-7: Material Impact Response Design Curves (with error bars)	66
Figure 5-1: CEAST 9340 Drop Tower (© Stephen Kimanzi)	70
Figure 5-2: Supporting Steel Plate(© Stephen Kimanzi)	71
Figure 5-3: Sample Drop Tower Impact Response for Sorbothane	73
Figure 6-1: Viscous Impact Model Response Prediction.....	96

List of Symbols

E	Young's Modulus of Elasticity
$E' & M'$	Storage modulus
$E'' & M''$	Loss modulus
E_o	Instantaneous modulus in a K-V based SLS model
E_K	Elemental modulus in a K-V based SLS model
E_M	Elemental modulus in a M-W based SLS model
E_∞	Long term modulus in a M-W based SLS model
$\sigma(t)$	Time dependent compressive axial stress
$\sigma^*(j\omega t)$	Complex dynamic stress
$\sigma_S; \sigma_D$	Spring stress; Dashpot stress in a viscoelastic model
$\varepsilon(t)$	Time dependent compressive axial strain
$\varepsilon^*(j\omega t)$	Complex dynamic strain
$\varepsilon_S; \varepsilon_D$	Spring strain; Dashpot strain in a viscoelastic model
η	Viscosity
η_K	Elemental viscosity in a K-V based SLS model
η_M	Elemental viscosity in a M-W based SLS model
$M(t)$	Stress relaxation modulus in compression
$M^*(j\omega)$	Complex dynamic modulus
$C(t)$	Creep function in compression
∂_t	Partial differential operator
τ_r	Stress relaxation time constant
τ_c	Creep constant
$H(t)$	Heaviside operator
$e^{j\theta}$	Euler's operator
$\tan \delta$	Loss factor (abbreviated as l_f in some instances)
k	stiffness
c	damping coefficient
ζ	Damping ratio
F_e	DMA stiffness correction factor
L	Thickness
A	Area in m^2
ω	External / causing frequency
ω_n	System natural frequency
m	mass
g	gravitational pull at $9.81 \frac{m}{s^2}$

List of Abbreviations

IED	Improvised Explosive Devices
TLD	Tuned Liquid Dampers
FFT	Fast Fourier Transform
MS – NS	Magnetic Spring with Negative Stiffness
TBI	Traumatic Brain Injuries
ASTM	American Society for Testing and Materials
EPS	Expanded Polystyrene
HIC	Head Injury Criterion
M-W	Maxwell-Wiechert
K-V	Kelvin-Voigt
SLS	Standard Linear Solid
EOM	Equation of Motion
DMA	Dynamic Mechanical Analyzer
LVDT	Linearly Variable Differential Transformer
LVR	Linear Viscoelastic Range
CAI	Compression After Impact
TPE	Thermoplastic Elastomer

Acknowledgements

I offer my enduring gratitude to the faculty, staff and my fellow students at UBC who have inspired me to continue my work in Engineering. I owe particular thanks to Dr. Seethaler, whose penetrating questions taught me to question more deeply. I thank Dr. Mohammadi for challenging my understanding of viscoelastic material science and providing coherent answers to my endless questions and Dr. Abbas Milani for his guidance on the field of material selection.

I thank Mr. Russell LeMountain for his support and advice for my experiments, and Mr. Bryn Crawford for instrumentation and experimental design knowledge. My sincerest gratitude to UBC Okanagan and Helios for their financial support throughout my education.

Special thanks are owed to my family and friends, whose have supported me throughout my years of education.

Dedication

Dedicated to my mother and father Christine and George, my brothers Simon and David, and to my best friend Muriel.

Chapter 1: Introduction

Engineering materials have a range of desirable properties useful in different applications. In modern day designs, selecting the right material is vital in maintaining reliability and minimizing cost. This is evident when dealing with non-classical materials whose behavior is affected by external factors and application conditions which is the case with viscoelastic materials. Viscoelastic materials have found increased use in the energy absorption industry due to their passive energy dissipation abilities [1]. The complexity of analysis due to their non-classical behavior of viscoelastic materials [2] make it challenging to devise a selection technique that can rank materials on their performance. This chapter will define the application parameters and explain fundamental material concepts used in the rest of the study. These definitions are important in making scientifically sound assumptions that we can use to create useful selection techniques through mathematical analysis. The thesis organization is presented at the end in Chapter 1.3.

1.1 Application Definitions

Energy dissipation is a common challenge in engineering whether in static or dynamic systems. Often, the target is not reducing the energy directly but one of its effects manifested in the form of displacement, velocity, or acceleration. The variable of analysis, in material selection, depends on the application so it is important to understand the scenarios where variables are significant. The application of focus in this research is impact absorption.

1.1.1 Impact Absorption

When an object moving with an initial velocity is forced to come to a complete stop, there is an associated deceleration which depends on the time taken to reduce the velocity to zero. For safety critical situations, the developed g-force during deceleration increases the potential severity of harm. Impact absorption is defined as the reduction of developed g-force by attenuating the energy on impact and increasing the time taken for the object to come a complete stop consequently decreasing the developed g-force during impact.

1.2 Viscoelastic Materials Definitions

Classical materials are broadly described by a binary system of elastic and viscous materials. For an elastic material, an application of stress produces a linearly related strain based on the material modulus. This is commonly referred to as Hookean behaviour [3]. For a viscous fluid, often referred to as a Newtonian fluid [3], the stress is linearly related to the strain rate based on the material viscosity.

In practice, purely elastic or viscous behaviour is not observed and often materials exhibit a combination of both properties and the dominant behaviour is considered the material behaviour. This is regularly sufficient to describe and model the material behaviour but there are situations where the influence of both elastic and viscous properties is significant such that classifying the material as purely viscous or elastic drastically misrepresents the behaviour. This is the case for viscoelastic materials as they exhibit both viscous and elastic behaviour depending on the loading parameters such as strain rate, temperature, peak load and so on.

Viscoelastic materials deform under load and transmit forces in all directions and may regain some if not all of their original shape once the load is removed. Moreover, some of the input energy is expelled as heat meaning that the transmitted load is less than the input load. This makes them excellent for impact absorption, vibration damping, and blast attenuation. Furthermore, the subgroup of viscoelastic materials that regain their shape when the load is removed can undergo cyclic loading with minimum fatigue which is a key factor in vibration isolation. The combined energy dissipation and vibration isolation makes them optimizable vibration dampers and isolators as opposed to using spring isolation systems or oil damping systems independently.

The science of viscoelastic materials and the modelling techniques are covered in depth in Chapter 2.

1.3 Thesis Organization

The aim of this thesis is to present a systematic approach for viscoelastic materials selection used in impact absorption. This will be done by modeling an impact of a mass on a viscoelastic material and making use of the Ashby method for material selection to creating the material indices. The resulting index will define the important material parameters for impact absorption and rank the 4 materials available for analysis which are Rubber, Sorbothane, Neoprene, and Santoprene.

A review of viscoelastic material use in vibration isolation and blast attenuation is presented in Chapter 2 to highlight the versatility of these materials but the main focus remains their use in impact absorption. The thesis outline is described below.

- Chapter 2 reviews solutions that have been applied thus far to mitigate vibration isolation, impact absorption, and blast attenuation and the opportunity for viscoelastic material based solutions. This chapter also reviews of viscoelastic material science including modeling and gives an overview of the Ashby material selection method.
- Chapter 3 introduces the impact absorption model and the formulation of the Ashby equations for different design scenarios.
- Chapter 4 presents the experimental work using Dynamic Mechanical Analysis and uses the performance index to create impact absorption design curves.
- Chapter 5 discusses drop tower validation experiments conducted to qualify the results of the material selection and assesses the impact of the modeling techniques and assumptions made to create the design curves.
- Chapter 6 summarizes the results of this research and its contributions to the field of viscoelastic material selection and impact absorption analysis.

Chapter 2: Literature Review

The presence of unwanted energy in Engineering applications is a common challenge in modern day designs. When unaccounted for, this energy could lead to fatal outcomes such as the collapse of The Tacoma Narrows bridge when it resonated and eventually failed catastrophically [4]. A combination of design strategies and material choices influence product performance, especially in dissipating unwanted energy. One common source of unwanted energy in a system is induced vibrations at varying frequencies which could cause resonance if they match the system's natural frequency. Therefore, it is in the interest of the designer to account for potential excessive energy in the system and develop strategies for dissipation. For effective strategy application, a clear understanding of energy dissipation methods and the required materials is important. This chapter covers energy dissipation in mechanical systems and describes the fundamentals of viscoelastic materials and the modeling techniques as well the properties that make them ideal for energy dissipation. Finally, a brief review of the Ashby method of material selection and its applicability in this analysis is presented.

2.1 Energy Dissipation in Mechanical Systems

The law of conservation of energy dictates that the energy of an isolated system remains constant with time. This means that energy cannot be destroyed or created but only transformed from one form to another. Therefore, energy dissipation is best defined as the transformation of mechanical energy to most commonly, heat energy, which is removed from the system by various mechanisms.

Generally, the notion is that energy dissipation is limited to removing energy for the purposes of safety. This is commonly seen in vibrating systems where induced vibrations can be catastrophic. However, there are instances where induced vibrations are desirable such as shake tables and concrete mixers. In the design of shaker tables [5], the materials used must withstand the operating frequency and amplitude of vibration range to avoid system failure. Moreover, since it would be counterintuitive to damp the induced vibrations to avoid resonance, the design and material choice play a significant role in proper performance.

Therefore, proper design measures to account for energy dissipation are not only useful for system performance and longevity, they are also safety critical in some instances. Often, observable vibration frequencies are considered when discussing energy dissipation but impact absorption is another area of study where an excess amount of energy must be dissipated from a system within an incredibly short amount of time. There is a significant amount of studies in sports science concerning the impact of sporting surfaces [6]–[8] with majority of the focus on footwear and their biomechanical impacts on cushioning the heel from impact during activities. While there is an expanse area for studying energy dissipation, this study will focus on devising a simple approach on the application of energy dissipation techniques in impact absorption.

2.1.1 Impact Absorption

When an object in motion comes to a stop against a surface, the kinetic energy is either absorbed within the system or dissipated. The rate at which the object comes to rest is called its deceleration and it depends on its initial velocity of travel plus its mass as well as the characteristics of the stopping surface. As the object comes to rest, the kinetic energy is dissipated through elastic or plastic deformation of stopping surface and the object. Typically, the softer the stopping surface the larger the deformation and consequently the lower the contact force developed between the object and the stopping surface thus lower deceleration values. Sometimes the energy dissipated by the stopping surface is insufficient and the contact force on the object is too high increasing the risk of failure. By maximizing the amount of energy dissipated by the stopping surface on impact, the impact force on the object is reduced and so is the risk of failure. In other words, impact absorption aims to minimize the contact force on the object by minimizing the deceleration of the system. The energy is absorbed through damping which reduces the amplitude of impact and alters the transmitted frequencies which reduces the risk of injury or completely eliminates it. The energy absorbed depends on the properties of the damping surface and can be maximized by optimal design and material selection. The ability of viscoelastic materials to deform under load and dissipate the energy makes them ideal for these applications.

In helmet design, the use of energy absorbing materials is ubiquitous. This is partly due to recent studies showing increased adverse traumatic brain injuries (TBI) experienced when motorists are involved in accidents [9]. TBIs range from mild concussive events to near fatal injuries common in vehicle accidents [2, 3]. To combat the occurrence of adverse TBIs, helmet design standards such as ASTM F1447 and Snell B-95 used in [12] outline the testing requirements and define the performance

criterion. Figure 2-1 shows the main design components of a helmet where the liner's function is to protect the wearer's head by absorbing the force transmitted through the outer shell [12].

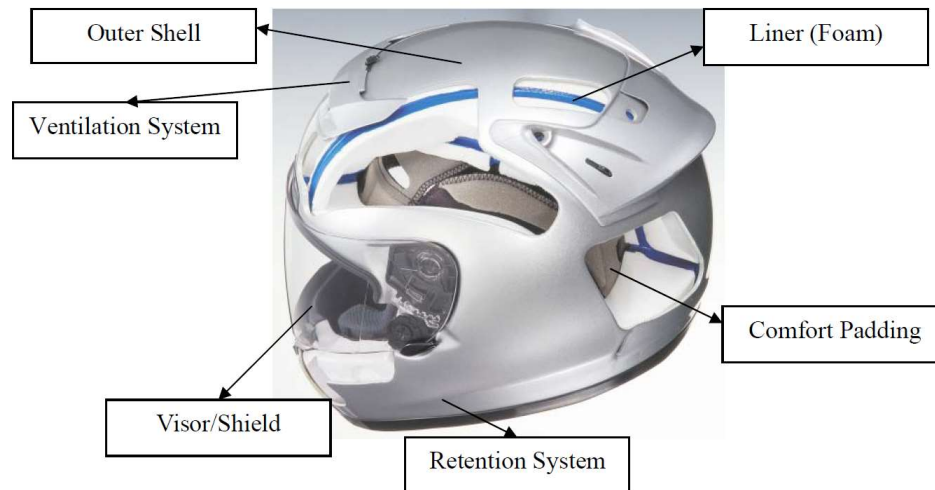


Figure 2-1: Helmet Parts [33]

The liner is made of a high impact absorbing material which is commonly Expanded Polystyrene (EPS). EPS characteristics allow for high impact absorption which reduces the potential for severe head injury. The performance of a helmet is quantified by the Head Injury Criterion (HIC) which is given by Equation 2-1. The time interval in Equation 2-1 is typically limited to a maximum of 36 ms to avoid extreme accelerations occurring over a long period. The term $a(t)$ is the acceleration of the head measured in g's (with respect to gravitational pull). The reason acceleration is measured is to determine how much above the tolerable g-force the induced acceleration is on the head. If the time interval is short, a higher acceleration may be acceptable since the resulting HIC is low.

$$HIC = \max \left\{ \left[\frac{\int_{t_1}^{t_2} a(t) dt}{t_2 - t_1} \right]^{2.5} (t_2 - t_1) \right\} \quad (2-1)$$

The HIC must be less than 1000 for a given time interval $t_1 \rightarrow t_2$ depending on the material. The acceleration and time of impact can both be controlled by the liner properties and the added effect of the helmet shell and other components can be factored in for overall design performance. Since the helmet's overall mass is constrained for user comfort [12], the choice of liner and geometry is critical. Traditionally, the liner is selected through a series of experimental procedures which vary geometric parameters for different material samples until a desired result is found [12]. While effective, this technique requires dedicated setup for the test rig and is time consuming when a variety of materials are available for testing. Creating a design equation that accounts for both material energy absorption and mass improves the process of liner selection and allows for rapid design.

Impact absorption is also widespread in the design of foot wear and high performance cushioning surfaces. In sporting events, a variety of surfaces such as concrete, asphalt and synthetic materials are used [7]. This variability in surface hardness alters the cushioning available to users and it has been suggested that this may lead to development of injuries over time such as shin splints and stress fractures [8]. The common notion is that stiffer surfaces are detrimental to users as they provide less absorption but that is not always the case [7]. The degree of impact absorption depends on the interaction of the user and the absorption surface. Factors like user mass, foot wear and nature of contact affect the level of cushioning provided by the surface. Dixon and Stiles' [7] work on impact absorption based on different shoe-surface combination revealed an array of factors such as surface material and thickness, shoe type, and athlete mass. In order to decide the correct surface and shoe combination, biomechanical analysis of the human body considers the development of fatigue injuries

based on the cushioning available. Each combination of mass and shoe type favours a different surface and characterizing all combinations is experimentally intensive. The availability of an impact absorption material selection equation minimizes the experimental work to individual material characterization and an optimal material for each situation can be readily determined.

The use of impact absorbing materials is also widespread in the shipping industry. With companies shifting to online based platforms, shipping and delivery services such as Amazon, UPS, and FedEx make use of cushioning materials to protect products from damage during shipping and handling. The most common type of cushioning material is expanded polystyrene (EPS) with widespread use in electronic components shipping. Polythene products are also commonly used infused with air pockets to create a cushioning effect when impact is experienced. However, the amount of polythene or EPS product used for cushioning can be unnecessarily bulky and with little after use when shipping is completed, the product waste is environmentally unreasonable [13],[14]. With a better understanding of cushioning requirements and an easier selection technique, both suppliers and consumers stand a chance of reducing both waste and cost.

Based on the literature presented above, it is evident that the common notion that softer materials provide better cushioning is fundamentally misleading because the performance of a cushioning material depends on intrinsic material properties and physical parameters such as drop height and mass. These factors make selection of an impact absorbing material in various applications a challenge when various options are available and intensive experimental work is required to quantify their performance. By incorporating all variables in a selection equation to account for application parameters, there is an opportunity to select the right material for different scenarios.

The use of viscoelastic materials in impact absorption is not limited to helmets, athletic surfaces, and packaging for shipments. Chapter 2.2 further highlights their versatility including the aspects that make them adaptable to multiple applications where energy absorption is required.

2.2 Viscoelastic Materials

In classical mechanics, an elastic material is one that responds to the application of stress σ by producing a strain ϵ linearly related to stress by the material's modulus of elasticity E . This is the behaviour of a Hookean solid [3] typically represented by Equation 2-2.

$$\sigma = E * \epsilon \quad (2-2)$$

Similarly, a purely viscous or Newtonian fluid responds to an applied stress σ based on Trouton's Law in Equation 2-3 [2]. The applied stress induces a time dependent strain, classified by the strain rate $\frac{d\epsilon}{dt}$ and the constant of proportionality to stress is called the viscosity η .

$$\sigma = \eta * \frac{d\epsilon}{dt} \quad (2-3)$$

Most engineering materials deviate from the binary classification of either purely elastic or purely viscous by exhibiting a combination of viscous and elastic behaviours. This combination is termed as Viscoelastic and is characterized by a time dependency between stress and strain. Other common pertinent definitions of non-classical behaving materials are summarized in Table 2-1.

Table 2-1: Non-classical Material Behavior

Viscoelastic	Materials exhibit both viscous and elastic behaviour and the stress experienced depends on both strain and strain rate.
Viscoplastic	Materials behave similar to viscoelastic materials with the key difference being the existence of a yield stress. From a rheological perspective, viscoelastic materials deform instantaneously under stress while viscoplastic materials do not deform until the yield stress is reached.
Hyperelastic	Materials have a stress-strain relationship derived from the strain energy density function and are a special case of Cauchy Elastic material since they are conservative i.e. stress causes large deformation.

The behaviour of complex non-classical materials has been explained in various rheological formulations based on observed experimental responses. Table 2-2 lists the various models used for each category presented in Table 2-1. There are many more models available in common literature used to describe complex material behaviour and the choice is often based on which model best describes the material being studied. Often, the more accurate a model the higher its complexity.

Table 2-2: Non-classical Materials Rheological Models

Viscoelastic	<ul style="list-style-type: none">• Maxwell-Wiechert• Kelvin-Voigt• Standard Linear Solid
Viscoplastic	<ul style="list-style-type: none">• Norton-Hoff• Bingham-Norton
Hyperplastic	<ul style="list-style-type: none">• St. Venant-Kirchhoff• Ogden• Mooney-Rivlin

This research is focussed on the phenomenological models of viscoelastic materials named above which include the Maxwell-Wiechert, Kelvin-Voigt, and the Standard Linear Solid. All viscoelastic materials are known to exhibit two primary behaviours namely creep and stress relaxation which are defined below. The degree to which a viscoelastic model represents creep and stress relaxation determines how well the model performs in representing viscoelastic material behaviour.

- I. **Creep** – when subjected to a constant initial stress, σ_0 , viscoelastic materials show an increase in strain with time [3]. This behaviour is depicted in Figure 2-2 below based on the standard linear solid model of viscoelastic materials.
- II. **Stress relaxation** – when subjected to a constant initial strain, ε_0 , viscoelastic materials exhibit a time-dependent stress decrease [3]. Figure 2-3 graphically represents the stress relaxation behaviour based on the standard linear solid model of viscoelastic materials.

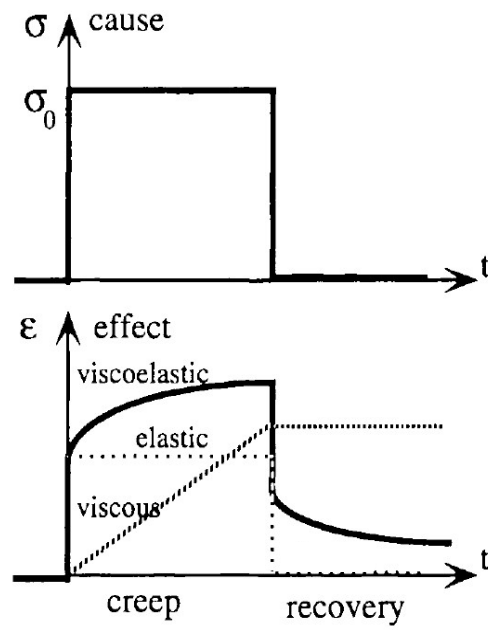


Figure 2-2: Standard Linear Solid Creep-Recovery Curve

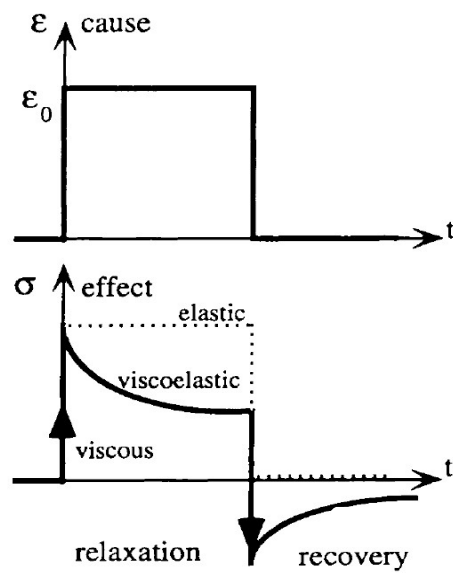


Figure 2-3: Standard Linear Solid Stress Relaxation-Recovery Curve

The rheological models for viscoelastic materials in Table 2-2 are typically modeled as a combination of springs and dashpots to represent the elastic and viscous components of viscoelastic material behaviour respectively. Each model has its own merits and detractions depending on the application and material being modeled. The individual model design and response analysis is discussed below

2.2.1 Maxwell-Wiechert Fluid Model

The first basic model of a viscoelastic material consists of a spring and a dashpot element connected in series shown in Figure 2-4 known as the Maxwell-Wiechert (M-W) model. When a force is applied, an equal stress is developed in both elements of the model but the individual strain depends on the constant on its response to an applied stress. The spring element responds with respect to its elastic modulus E and the dashpot element responds based on its viscosity η with the rate of deformation.

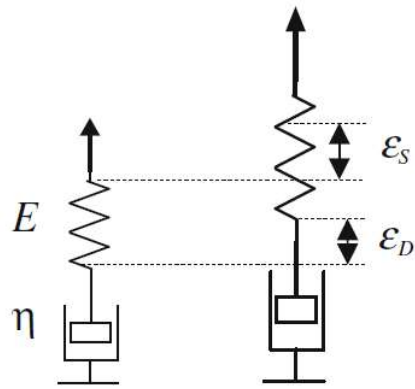


Figure 2-4: Maxwell-Wiechert Fluid Model

The total strain on the system is an addition of the elemental strains which is described by Equation 2-4 and is the constitutive equation for a single element Maxwell-Wiechert model. This is the response of a typical fluid hence the M-W model is often described as a fluid model [3].

$$\boldsymbol{\varepsilon}(t) = \frac{\boldsymbol{\sigma}(t)}{E} + \frac{1}{\eta} \partial_t \boldsymbol{\sigma}(t) \quad (2-4)$$

Using the M-W model for analysis requires understanding its response to an input strain or stress to study its creep and stress relaxation behaviour. By mathematically simulating its response under load using the constitutive equation, we can identify its merits and shortcomings for different applications.

For the stress relaxation response, we subject the model to a general input strain described by Equation 2-5 where $f_1(t)$ describes a particular strain and the material stress response is given by Equation 2-6 obtained by evaluating Equation 2-4 with the strain as the controlled variable.

$$\boldsymbol{\varepsilon}(t) = f_1(t)H(t - t_o) \quad (2-5)$$

$$\boldsymbol{\sigma}(t) = E \cdot \boldsymbol{\varepsilon}(t_o^+) \cdot e^{-(t-t_o)\tau_r} + \int_{t_o}^t E \cdot e^{-(t-s)\tau_r} \frac{d\boldsymbol{\varepsilon}}{dt} ds; \tau_r = \frac{\eta}{E} \quad (2-6)$$

The stress relaxation modulus for a M-W model can be obtained by considering the strain in Equation 2-5 as a step strain described by Equation 2-7.

$$\boldsymbol{\varepsilon}(t) = \boldsymbol{\varepsilon}_o H(t - t_o) \quad (2-7)$$

The resulting stress equation from this calculation is divided by the constant step strain to obtain the stress relaxation modulus $M(t)$ in Equation 2-8 with $\tau_r = \frac{\eta}{E}$ as the characteristic stress relaxation time [3]. The stress relaxation behaviour of the M-W model is graphically represented in Figure 2-5a which resembles the standard behaviour of a viscoelastic material shown in Figure 2-3. This makes the M-W model useful when studying applications that involve viscoelastic stress relaxation behaviour. These applications typically occur over a long period of time.

$$M(t) = \frac{\sigma(t)}{\epsilon_o} = E \cdot e^{-\frac{t}{\tau_r}} \quad (2-8)$$

For the creep behaviour analysis of the M-W model to an input stress, we first rearrange the characteristic equation as shown in Equation 2-9 to obtain the strain response. This is because each element in the M-W model experiences a unique strain value but the stress is similar.

$$\frac{d}{dt}\epsilon(t) = \frac{1}{E} \cdot \frac{d}{dt}\sigma(t) + \frac{1}{\eta} \cdot \sigma(t) \quad (2-9)$$

For a general input stress defined by Equation 2-10, the response is obtained by manipulating Equation 2-9 which results into Equation 2-11.

$$\sigma(t) = f_2(t)H(t - t_o) \quad (2-10)$$

$$\epsilon(t) = \frac{1}{E} \cdot \sigma(t_o^+) + \int_{t_o}^t \sigma(s) ds \quad (2-11)$$

The creep response of the M-W model is obtained for a step stress given in Equation 2-12 and by simplification we obtain the creep $\mathcal{C}(t)$ given by Equation 2-13. In Figure 2-5b, the creep behaviour of a M-W model is linearly increasing with time implying that it increases infinitely over time. Moreover, the removal of the applied force sees the material response instantaneously fall to a constant residual strain which contradicts the standard response of viscoelastic materials in Figure 2-2. This is a known short-coming of the M-W model and must be considered when used in modeling.

$$\sigma(t) = \sigma_o H(t - t_o) \quad (2-12)$$

$$\mathcal{C}(t) = \frac{\varepsilon(t)}{\sigma_o} = \left[\frac{1}{E} + \frac{t}{\eta} \right]; t > 0 \quad (2-13)$$

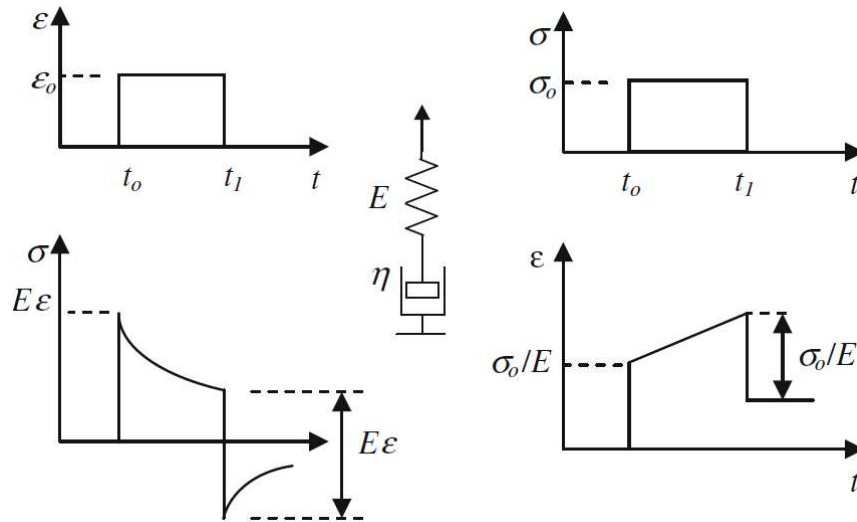


Figure 2-5: Maxwell-Wiechert Stress relaxation (a) and Creep (b) responses

2.2.2 Kelvin-Voigt Solid Model

The M-W model combines the basic elements in series and has been shown to fall short in describing viscoelastic creep behaviour. In an attempt to accurately represent material creep, the Kelvin-Voigt (K-V) model arranges the basic elements in parallel shown in Figure 2-6.

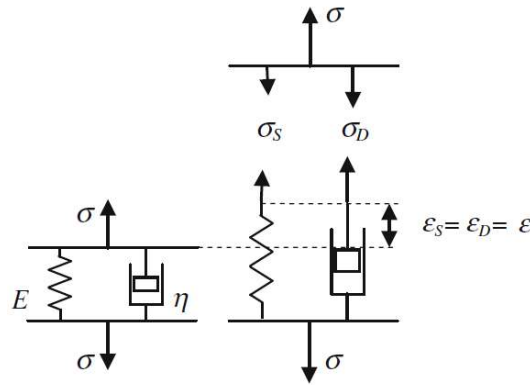


Figure 2-6: Kelvin-Voigt Solid Model

When a force is applied to this model, both elements compress equally which translates to an equal strain ϵ . Therefore, the total stress is an addition of individual stresses controlled by the spring stiffness E and the dashpot viscosity η resulting into the K-V constitutive equation is given by Equation 2-14.

$$\sigma(t) = (E + \eta \cdot \partial_t)\epsilon(t) \quad (2-14)$$

In a similar fashion to the M-W mode, the stress relaxation and creep functions for the K-V model are determined. For the stress relaxation behaviour, we begin by subjecting the model to a general input strain given by Equation 2-15 and the resulting stress response is obtained by evaluating the constitutive equation which is given by Equation 2-16.

$$\boldsymbol{\varepsilon}(t) = f_3(t)H(t - t_o) \quad (2-15)$$

$$\boldsymbol{\sigma}(t) = E \cdot f(t) \cdot H(t - t_o) + \eta \cdot [H(t - t_o) \cdot \frac{d}{dt}f(t) + f(t_o)\delta(t - t_o)] \quad (2-16)$$

Considering a step strain for Equation 2-15 in the form of $f(t) \equiv \varepsilon_o$, the stress relaxation modulus is given in Equation 2-17. In Figure 2-7a, the K-V model stress relaxation plot represents an instantaneous response with a constant value during the duration of the strain before instantaneously reverting to the original point when the strain is removed. This differs from the standard viscoelastic material response in Figure 2-2 and is a known shortcoming of the K-V model [3].

$$M(t) = \frac{\boldsymbol{\sigma}(t)}{\varepsilon_o} = E \cdot H(t) + \eta \cdot \delta(t) \quad (2-17)$$

For creep behaviour, the constitutive equation is rewritten with respect to strain in Equation 2-18.

$$\frac{d}{dt}\boldsymbol{\varepsilon}(t) + \frac{E}{\eta} \cdot \boldsymbol{\varepsilon}(t) = \frac{\boldsymbol{\sigma}(t)}{\eta} \quad (2-18)$$

The strain response for a general input stress defined by Equation 2-19 is given by Equation 2-20.

The creep constant τ_c , also called a retardation constant, is a material specific behaviour describing its response under load and determines when the material begins to creep.

$$\sigma(t) = f_4(t)H(t - t_o) \quad (2-19)$$

$$\varepsilon(t) = H(t - t_o) \cdot \int_{t_o}^t e^{-\frac{t-s}{\tau_c}} \cdot \frac{f(s)}{\eta} ds; \tau_c = \frac{\eta}{E} \quad (2-20)$$

Finally, the creep function for a K-V model based on a step stress $f(t) \equiv \sigma_o$ is given by Equation 2-21. The creep behaviour of a K-V model is presented Figure 2-7b which agrees with the standard behaviour of a viscoelastic material presented in Figure 2-2.

$$C(t) = \frac{\varepsilon(t)}{\sigma_o} = \frac{\left[1 - e^{-\frac{t}{\tau_c}}\right]}{E}; t > 0 \quad (2-21)$$

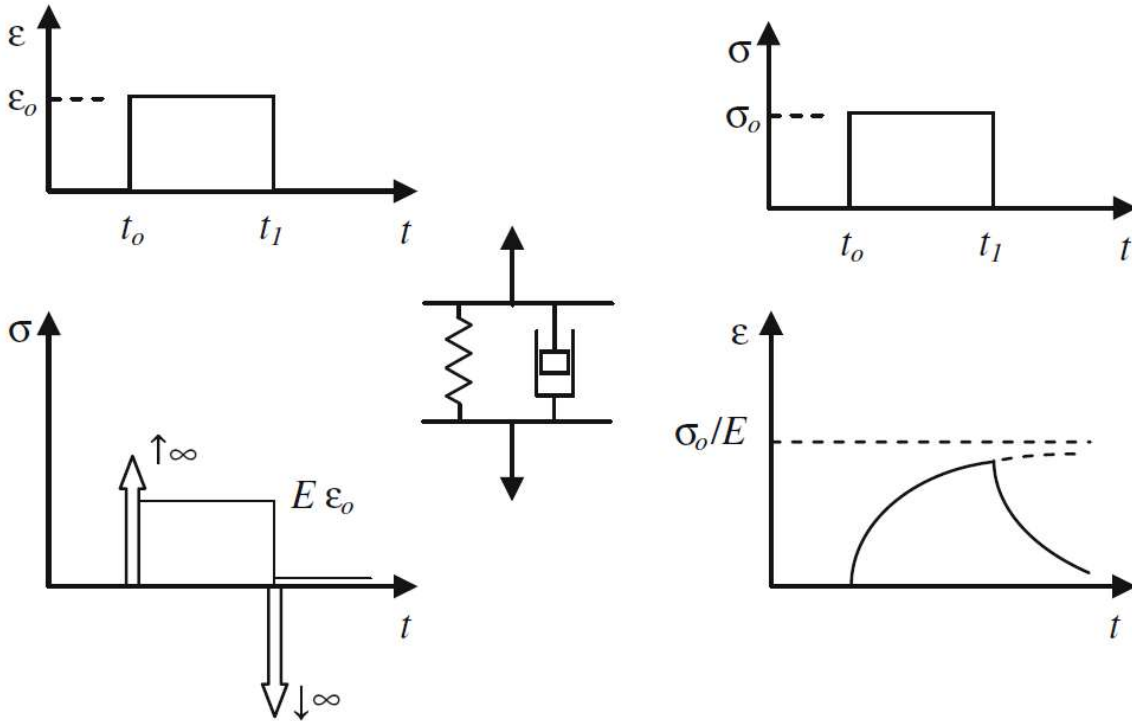


Figure 2-7: Kelvin-Voigt Model Stress relaxation (a) and Creep (b) Responses

The Kelvin-Voigt stress relaxation response in Figure 2-7a shows instantaneously high stresses that tend toward infinity. This is because once a deformation is applied, the dashpot stiffens up and behaves like a complete solid reacting to the input deformation by resisting any deformation.

2.2.3 Standard Linear Solid

The M-W and K-V models have been unable to fully describe the creep and stress relaxation behaviour of viscoelastic materials thus far. It has been shown that by adding an extra element to either of these models, either model can completely represent the behaviour of viscoelastic materials [2]. This can be achieved either by adding a spring in series with the K-V model shown in Figure 2-8a or a spring in parallel with the M-W model as shown in Figure 2-8b. These are the two variations of the Standard Linear Solid (SLS) and it is not important which model is used in the derivation of the SLS response since there is a mathematical equivalence between the models [3]. The analysis presented here uses the spring in series with a K-V model to generate the SLS response.

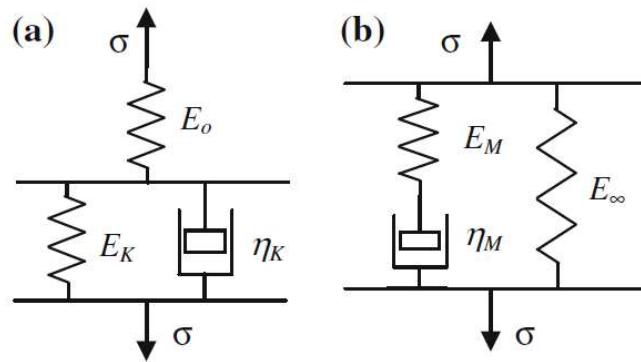


Figure 2-8: Standard Linear Solid using K-V (a) and M-W (b)

When a force is applied to the SLS model in Figure 2-8a, the spring and the K-V unit experience a similar stress but different strains and the elements of the K-V unit deform similarly under different stresses. Combining the two portions, the resulting constitutive equation is given by Equation 2-22.

$$(\mathbf{E}_o + \mathbf{E}_k)\boldsymbol{\sigma}(t) + \boldsymbol{\eta}_k \cdot \frac{d}{dt}\boldsymbol{\sigma}(t) = (\mathbf{E}_o\mathbf{E}_k) \cdot \boldsymbol{\varepsilon}(t) + (\mathbf{E}_o\boldsymbol{\eta}_k) \cdot \frac{d}{dt}\boldsymbol{\varepsilon}(t) \quad (2-22)$$

Equation 2-22 contains multiple variables which make it challenging to calculate the model response to any input. For simplicity, we introduce general rheological operators based on the work in [3] and this results into Equation 2-23.

$$\mathbf{p}_o\boldsymbol{\sigma} + \mathbf{p}_1 \cdot \frac{d\boldsymbol{\sigma}}{dt} = \mathbf{q}_o\boldsymbol{\varepsilon} + \mathbf{q}_1 \cdot \frac{d\boldsymbol{\varepsilon}}{dt} \quad (2-23)$$

These operators are summarized in Table 2-3.

Table 2-3: Equivalent SLS Model Rheological Operators

Operator	Equivalent Term
p_o	$E_o + E_k$
p_1	η_k
q_o	$E_o E_k$
q_1	$E_o \eta_k$
τ	$\frac{p_1}{p_o}$
λ	$\frac{q_1}{q_o}$

Equation 2-23 is modified to Equation 2-24 to study the strain response of the SLS. For a general input strain described by Equation 2-25, the response of the SLS model based on the behaviour described for Figure 2-8a is represented by Equation 2-26.

$$\frac{d\sigma}{dt} + \frac{1}{\tau}\sigma = \frac{q_o}{p_1}\varepsilon + \frac{q_1}{p_1} \cdot \frac{d\varepsilon}{dt} \quad (2-24)$$

$$\varepsilon(t) = f_5(t)H(t - t_o) \quad (2-25)$$

$$\sigma(t) = H(t - t_o) \int_{t_o}^t e^{-\frac{t-s}{\tau}} \left[\frac{q_o}{p_1} f(s) + \frac{q_1}{p_1} \cdot \frac{df(s)}{ds} \right] ds + \frac{q_1}{p_1} e^{-\frac{t-t_o}{\tau}} \cdot f(t_o) \quad (2-26)$$

We can determine the stress relaxation modulus of the SLS model by considering a step strain input in Equation 2-25 and simplifying Equation 2-26 by dividing through with a step strain $f(t) \equiv \varepsilon_o$. The result is the SLS model stress relaxation modulus equation given by Equation 2-27 and graphically represented by Figure 2-9. The graphical representation matches the standard behaviour of viscoelastic materials in Figure 2-2 which is advantage of using the SLS model.

$$M(t) = \frac{q_o}{p_o} + \left[\frac{q_1}{p_1} - \frac{q_o}{p_o} \right] e^{-\frac{t}{\tau}}, t > 0 \quad (2-27)$$

The stress relaxation behaviour of the SLS matches that of a standard viscoelastic material so intuitively, we must investigate whether its creep behaviour is representative of standard material behaviour. To do this, we first modify Equation 2-22 into Equation 2-28 to study the strain response.

$$\frac{d\varepsilon}{dt} + \frac{1}{\lambda}\varepsilon = \frac{p_o}{q_1}\sigma + \frac{p_1}{q_1} \cdot \frac{d\sigma}{dt} \quad (2-28)$$

For a general applied stress described by Equation 2-29, the strain response is described by Equation 2-30. The creep response is obtained by considering a step stress $f(t) \equiv \sigma_o$ and the resulting creep function is given by Equation 2-31.

$$\sigma(t) = f(t)H(t - t_o) \quad (2-29)$$

$$\varepsilon(t) = \left\{ \frac{p_o}{q_o} \left[1 - e^{-\frac{t-t_o}{\lambda}} \right] + \frac{p_1}{q_1} e^{-\frac{(t-t_o)}{\lambda}} \right\} H(t - t_o) \sigma_o \quad (2-30)$$

$$C(t) = \frac{p_o}{q_o} + \left[\frac{p_1}{q_1} - \frac{p_o}{q_o} \right] e^{-\frac{t}{\lambda}}, t > 0; \lambda \equiv \frac{q_1}{q_o} \quad (2-31)$$

The creep function for the SLS model is graphically represented in Figure 2-10 and resembles that of standard viscoelastic material response given in Figure 2-2. This makes SLS model the most accurate representation for viscoelastic materials when compared to M-W and K-V models. Notably, for all the improvements the SLS model introduces, it exhibits a horizontal asymptote (stabilization) when $t \rightarrow \infty$ but in practice, creep strain shows infinite increase with time [3]. Other complex models such as the Burgers models have been created to account for this behaviour and further accurately represent viscoelastic materials. This is a challenge when it comes to viscoelastic design because one can always create a better fitting model to better describe a material but often that requires increased computation power and may not translate to a significant improvement in design performance. It is often necessary to use simpler models because they are sufficient in describing the application without the additional computing power. For instance, the M-W model fails to describe creep behaviour in viscoelastic materials and the K-V model fails to properly represent stress relaxation behaviour. However, there are applications in which neither creep nor stress relaxation are a significant concern due to the time scale of interest and it is important to select a model that provides results without necessarily requiring complex formulations for material behaviour.

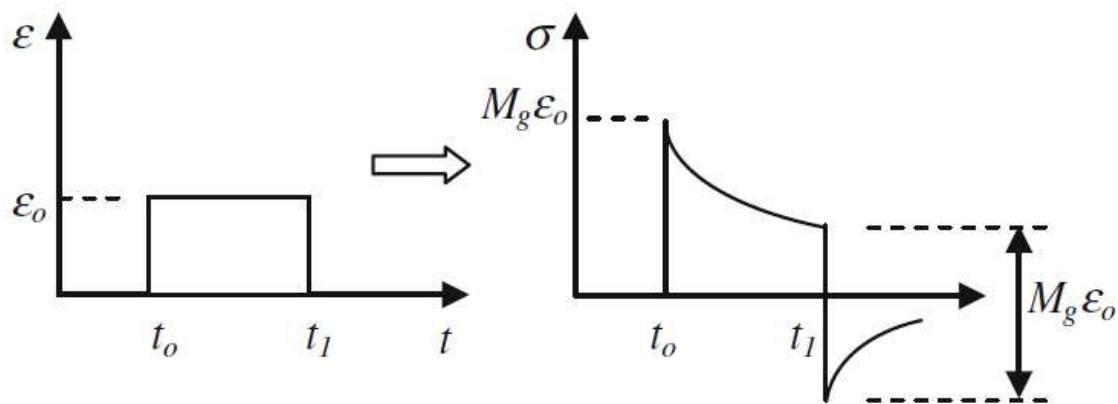


Figure 2-9: SLS Model Stress relaxation Behavior

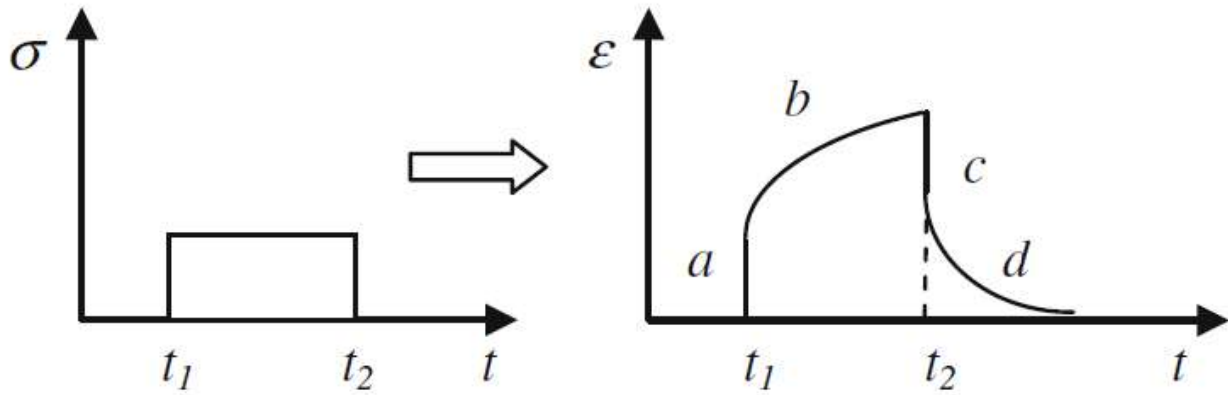
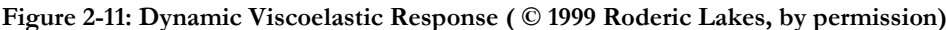


Figure 2-10: SLS Model Creep Behavior

The study of static viscoelastic material response is useful in determining which model best describes the material behaviour while properly describing creep and stress relaxation. However, the benefits of viscoelastic materials are seen in dynamic applications. Therefore, we will review their response under dynamic loads which is significant for the three cases introduced.

2.2.4 Viscoelastic Material Dynamic Behaviour

In addition to creep and stress relaxation behaviour, the behaviour of viscoelastic materials under dynamic loads is of engineering significance because the combination of elastic and viscous behaviour produces a phase lag between the load and response curves. This phase lag is important in design because describes the alteration of load transmission through the material and determines the amount of force registered on the back end of the material. Under a sinusoidal load, the load-displacement curve for a viscoelastic material produces an elliptical shape called a hysteresis loop [3] shown in Figure 2-11.



Studying the dynamic behaviour of viscoelastic materials is challenging when the models are described using the differential form of rheological equations. By transforming these equations into the frequency domain, relationships between material properties in the time domain and their complex counterparts can be derived. This is particularly useful for studying energy dissipation such as design for vibration damping or impact absorption since the load is dynamic and time dependent. This transformation also takes the integral or differential form of viscoelastic constitutive equation in the time domain and makes them simple algebraic expressions which are easier to work with in design. This transformation is explained in Chapter 2.2.4.1 and it is useful when rheological models describing the materials already exist. However, sometimes material models may not exist and it is important to experimentally determine the storage modulus and loss factor. This is described in Chapter 2.2.4.2.

2.2.4.1 Mathematical Loss and Storage modulus

When the material constitutive model is known, the response to any input can be predicted by simple mathematical manipulation. This includes the dynamic response to sinusoidal behaviour which uses Euler's formula in Equation 2-32 to represent the complex quantities.

$$e^{j\theta} = \cos \theta + j \cdot \sin \theta \quad (2-32)$$

Using Euler's formula, we can transform the applied strain to represent the complex strain with real and imaginary parts in Equation 2-33.

$$\varepsilon^*(j\omega t) \equiv \varepsilon_o e^{j\omega t} = \varepsilon_o [\cos \omega t + j \cdot \sin \omega t] \quad (2-33)$$

The resulting complex stress in Equation 2-34 is obtained by computing the complex integral using the material modulus equation which is found by solving the model's response to an input strain as described in Chapter 2.2. Appendix A.1 covers the derivations for linear viscoelastic material response which is used in Equation 2-34.

$$\sigma^*(j\omega t) = \varepsilon_o j\omega \int_{-\infty}^t M(t - \tau) e^{j\omega\tau} d\tau \equiv \left[j\omega \int_0^{\infty} M(u) e^{-j\omega u} du \right] \varepsilon^*(j\omega t) \quad (2-34)$$

Equation 2-34 can be written in terms of strain and modulus in Equation 2-35 showing that the steady state viscoelastic stress is directly proportional to the complex strain under harmonic excitation. The proportionality term, $M^*(j\omega)$, is called the complex modulus obtained by a Fourier transform of the stress relaxation modulus $M(t)$ in Equation 2-36.

$$\sigma^*(j\omega t) = M^*(j\omega) \varepsilon^*(j\omega t) \quad (2-35)$$

$$M^*(j\omega) = j\omega \int_0^{\infty} M(t)e^{-j\omega t} dt \quad (2-36)$$

In the study and characterization of viscoelastic material behaviour, it is common to express the complex modulus $M^*(j\omega)$ in its Cartesian form shown in Equation 2-37 and represent the quantities on the Argand plane as follows in Figure 2-12.

$$M^*(j\omega) = M'(\omega) + j \cdot M''(\omega) \quad (2-37)$$

The parameters M' and M'' are called the loss and storage modulus respectively and they represent the elastic and viscous components of the material's response. The storage modulus determines the amount of energy stored and the loss modulus describes the energy lost in a dynamic cycle [2]. In Figure 2-12, the angle δ_M is the phase difference between the two moduli and by definition, $\tan \delta_M$ is the ratio of the two moduli which describes the materials damping ability [2].

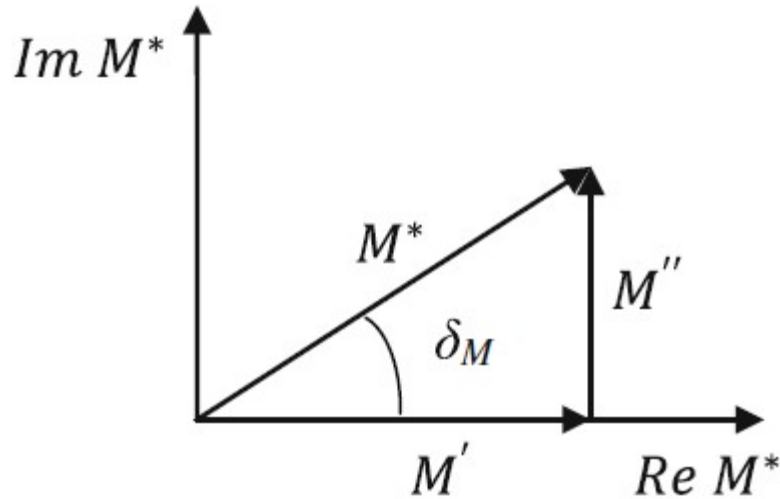


Figure 2-12: Viscoelastic Material Complex Modulus Argand Plane

Transforming to the frequency domain introduces dynamic properties that are key in studying cyclic applications. If the material's stress relaxation equation is known, we can determine the storage and loss moduli for varying frequencies. The storage and loss moduli based on the standard model stress relaxation equations introduced earlier are derived in the next subsections. Detailed derivations are provided in Appendix A.2.

2.2.4.1.1 Maxwell-Wiechert Fluid

In Chapter 2.2.1, the stress relaxation modulus for a single element M-W model was described by Equation 2-38 with τ_r defined as the characteristic stress relaxation time $\frac{\eta}{E}$. By Fourier transform, the storage and loss moduli for the single element M-W model are given in Equation 2-39. It is clear that both moduli are frequency dependent variables which is key when determining whether the M-W model accurately represents material behavior. The derivation is given in Appendix A.2.1.

$$M(t) = E e^{-\frac{t}{\tau_r}} \quad (2-38)$$

$$M^*(j\omega) = E \cdot \frac{(\omega\tau_r)^2}{1 + (\omega\tau_r)^2} + j \cdot E \cdot \frac{\omega\tau_r}{1 + (\omega\tau_r)^2} \quad (2-39)$$

2.2.4.1.2 Kelvin-Voigt Solid

The stress relaxation modulus for a K-V model in Chapter 2.2.2 was defined by Equation 2-40.

$$\mathbf{M}(t) = \mathbf{E} \cdot \mathbf{H}(t) + \boldsymbol{\eta} \cdot \boldsymbol{\delta}(t) \quad (2-40)$$

By Fourier transform, the storage and loss moduli for a single element K-V model is given by Equation 2-41 which shows that the storage modulus is frequency independent and the loss modulus is dependent on the material viscosity. The derivation for these moduli is given in Appendix A.2.2. In Chapter 2.22, the K-V model was shown to fall short in representing the stress relaxation behavior of viscoelastic materials and coupled with the indication that the storage modulus is a frequency independent behavior mathematically, the K-V model is further shown to be unreliable in representing viscoelastic stress relaxation behavior.

$$\mathbf{M}^*(j\omega) = \mathbf{E} + j \cdot \boldsymbol{\eta} \cdot \omega \quad (2-41)$$

2.2.4.1.3 Standard Linear Solid

In Chapter 2.2.4, the stress relaxation modulus for a single element SLS model was given by Equation 2-42.

$$M(t) = \frac{q_o}{p_o} + \left[\frac{q_1}{p_1} - \frac{q_o}{p_o} \right] e^{-\frac{t}{\tau}} \quad (2-42)$$

By Fourier transform, the resulting storage and loss moduli for the SLS are given by Equation 2-43 with the full derivation in Appendix A.2.3.

$$M^*(j\omega) = \frac{q_o}{p_o} + \left[\frac{q_1}{p_1} - \frac{q_o}{p_o} \right] \cdot \frac{(\omega\tau)^2}{1 + (\omega\tau)^2} + j \cdot \left[\frac{q_1}{p_1} - \frac{q_o}{p_o} \right] \cdot \frac{\omega\tau}{1 + (\omega\tau)^2} \quad (2-43)$$

The SLS model indicates that both moduli are frequency dependent variables but the challenge in using the SLS is the level of complexity involved in analysis which may not always translate into better material representation.

The stress relaxation models may not always exist for a given material and it is important to understand how to experimentally determine the storage and loss moduli based on fundamental measurable viscoelastic quantities. This is covered below.

2.2.4.2 Experimental Loss & Storage Moduli

Mathematically determining the storage and loss moduli requires prior existence of the stress relaxation modulus for a material. This is challenging when dealing with new materials because their behavior is unknown and thus having a model is unlikely. In such cases, experimentally determining the material behavior using raw signals is necessary. There is an array of equipment available for dynamic analysis such as the one used in this analysis discussed in Chapter 4 but all these instruments

are designed with different models and conditions in mind which often simplify the material behavior in order to produce measurements. By measuring raw signals, we can calculate the moduli for different materials while assuming different models and comparing them to the instrument measured quantities.

2.2.4.2.1 Maxwell Model

For a Maxwell model, Equation 2-44 describes the stress strain relationship in phasor¹ notation. Experimentally, we can measure the input force, F , and the resulting displacement, X , as well as the phase difference, δ , between them.

$$\epsilon = \left(\frac{1}{E} + \frac{j\omega}{\eta} \right) \sigma \quad (2-44)$$

The Argand diagram in Appendix A.3.1 represents the behavior of the M-W model and by representing stress and strain in their fundamental form using force, displacement, and area, the experimental storage and loss moduli for a M-W model are calculated using Equation 2-45 and Equation 2-46 respectively. The derivation is given in Appendix A.3.1.

$$E = \frac{F L_o}{A X} \frac{1}{\cos \delta} \equiv E' \quad (2-45)$$

$$\eta \omega = \frac{F L_o}{A X} \omega^2 \frac{1}{\sin \delta} \equiv E'' \quad (2-46)$$

¹ We make use of Phasor notation since it incorporates frequency which is a controlling parameter for dynamic analysis.

2.2.4.2.2 Kelvin Model

For a Kelvin model, Equation 2-47 describes the stress strain relationship in phasor notation. Once we experimentally determine the input force, F , and the resulting displacement, X , as well as the phase difference, δ , between them, we make use of the Argand diagram in Appendix A.3.2 and by fundamental definition of stress and strain, the storage and loss moduli for a K-V model are given by Equation 2-48 and Equation 2-49 respectively. The derivation for both parameters is given in Appendix A.3.2.

$$\sigma = (E + \eta j\omega)\epsilon \quad (2-47)$$

$$E = \frac{F L_o}{A X} \cos \delta \equiv E' \quad (2-48)$$

$$\eta\omega = \frac{F L_o}{A X} \sin \delta \equiv E'' \quad (2-49)$$

The SLS model is not a fundamental model and it is therefore challenging to relate experimental measurements to its parameter. For this reason, it is not covered in this Chapter.

2.2.5 Modelling Viscoelastic Materials

Chapter 2.21 to Chapter 2.24 introduced the various viscoelastic modeling techniques and analysis of their dynamic behaviour both mathematically and experimentally. However, the choice of model is left to the designer depending on the application at hand, material to be modelled and the desired degree of accuracy. Each model has its strengths and drawbacks so prematurely selecting a design model for all analysis techniques is a flawed approach.

2.3 Ashby Material Selection

Engineering materials are often used in components fulfilling multiple objectives like supporting a load without failure while being cheap, light, or meeting dimensional constraints[15]. These objectives are often contradictory and selecting the right materials comprises of advanced decision making and compromises as applications vary. With each application, constraints like dimension, minimum failure criteria, allowable stresses and strains vary and the material properties that satisfy a given design problem may fail once the design parameters change.

With the variety of engineering materials available, understanding the application helps narrow the family of materials the designer needs to consider. Then using property charts or characterization experiments, the desirable material properties can be determined and incorporated into the application calculations. Conventionally, there are six classes for engineering materials including polymers, ceramics, metals, glasses, hybrids, and elastomers[15]. In order to select the right material, the Ashby method of material selection is divided into sub sections that progressively result in selecting the optimal material.

2.3.1 Function

This identifies the requirement the design must fulfill whether it is to support a load, contain an amount of pressure, or absorb a required amount of energy [15]. In applications where specific performance numbers are unknown, an engineering description identifying the design conditions such as ties in tension or compression rods is provided. By properly defining the function, any design engineer can easily comprehend the design task being undertaken. For example, the design of pressure vessel would have a function defined as pressure vessel which automatically translates to a yield stress consideration if dealing with a yield-before-break design scenario.

2.3.2 Constraints

Once the design function is defined, fixed parameters that constrain the design must be listed. These constraints are often deterministic by the material selection stage and they vary from geometric constraints to failure modes [15]. For the pressure vessel design examples, the vessel radius and height are geometric constraints often specified because of space limitations and the failure mode, yield-before-break or leak-before-break determines whether the material's yield strength or its fracture strength is used in calculation. These constraints guide the material selection process by limiting the number of materials that can satisfy the function while meeting the set constraints.

2.3.3 Objective

In design, multiple materials end up fulfilling the function while meeting all constraints. A design objective is usually defined to ensure that the selected material meets all specifications while being the economically wise choice. For instance, when designing a pressure vessel, the objective can be set as minimizing mass which means the final material choice should produce the lightest pressure vessel possible. The objective is used to create the performance equation which is a combination of the function and constraints and material properties. Most designs have more than one objective in which case the designer decides the significance level of each objective and ranks the materials based on the combined performance in each objective category [15]. Other common objectives include minimizing cost or energy consumption per unit produced.

2.3.4 Free Variable

The parameters of the objective function include constrained geometric factors and variable elements that can be altered when fulfilling the objective. These are called free variables because they are left up to the designer's discretion. For material selection, the material choice is always a free variable. Free variables are essential in generating the objective function by making them the subject of the function equation and substituting them in the objective function. For example, in pressure vessel design, the wall thickness is unconstrained and forms part of the stress equation as well as the mass equation. By substitution, the mass of the vessel can be related to the stresses developed in the vessel which allows for material selection using the material yield strength (see Ch. 8 in [15]). The final performance equation only contains material properties as the free variable which are translated into the material index used in generating the performance curves. Parks and Clarkson [16] provide a detailed introduction and practical examples for material selection of a brake caliper and casing with multi-objective analysis.

In this study, Chapter 3 uses the Ashby Material selection technique to create the performance equation for impact absorption with some modifications to create readily applicable design selection curves. The Ashby method is convenient and simple to use but requires simplification of the situation to produce results so any assumptions made will be described within. It is a fundamental technique when quick decisions are to be made but further analysis of the design scenario is required once the initial material choice has been made.

Chapter 3: Design Equations

Impact absorption is a key area for viscoelastic material application as identified in Chapter 2. Moreover, there is an array of application potential that extend beyond synthetic viscoelastic materials to natural ones like human tissue and its response to impacts. This varied application base makes impact absorption a significant area of study and will be the main topic for analysis hereinafter. From Chapter 3.1 onwards, the focus is on modeling viscoelastic material behavior for impact absorption and experimentally validating the model results.

3.1 Impact Absorption

In Chapter 2, the goal of impact absorption was to reduce the magnitude of the transmitted force when an object in motion suddenly comes to a stop. The magnitude of transmitted force is determined by the deceleration such that in application, the parameter of interest is the maximum deceleration reached. The equivalent g-force developed during deceleration has been found to increase risk in brain injuries in neurological studies [10] and is also significant in determining cushioning materials performance [17]. Therefore, the primary objective of impact absorption is to minimize the maximum deceleration developed during impact.

The impact problem setup, objective and key assumptions are summarized in Table 3-1. Other assumptions are stated in text where necessary.

Table 3-1: Impact absorption problem definition

Description	An object of mass m impacts a material at a velocity v_0 . Determine the material properties that minimize the acceleration at the point of impact.
Objective	Minimize acceleration to a value below critical a_{max} .
Assumptions	Material mass and gravitational effects are negligible.

The impact of a viscoelastic material is modeled as a second order system in Figure 3-1. The free body diagram of the problem shows the mass M as the object whose acceleration is to be minimized and the variables k and c being are the equivalent stiffness and damping coefficient derived from a Kelvin-Voigt viscoelastic material model. The Kelvin-Voigt model is better suited to this application because its shortcoming is being unable to describe stress relaxation which is not a concern for impact analysis given the timeframe of interest is often in the millisecond timescale.

Predictive modeling such as that by Larson et. al [18] has been used to predict impact response of viscoelastic materials with good accuracy but is entirely experimental which requires a significant number of experiments to execute. Moreover, the predicted and experimental results were comparable for specific sample size to impactor ratios which further inhibits extrapolation to larger scale applications. In his modeling work, Argatov's [19] stipulates that the various viscoelastic models introduced in Chapter 2.2 have different dependencies to design parameter and that neither model is necessarily better than the other practically leaving the decision to the designer.

Evidently, viscoelastic modeling techniques are extensive and in their review paper, Zhou et. al [20] cover the various types of viscoelastic damping materials, modeling and experimental techniques currently in application based on present day research and is a recommended read for further information. In the present work, the analysis and methods used are based on Figure 3-1.

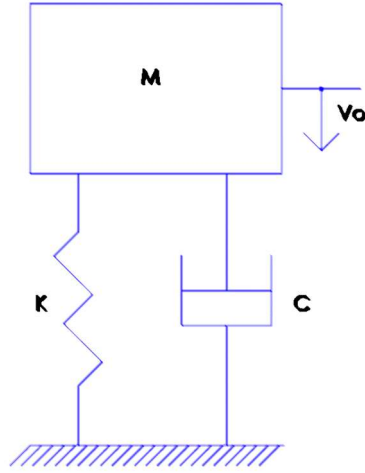


Figure 3-1: Second order model for Impact Analysis

The equation of motion (EOM) describing the viscous model in Figure 3-1 is given by Equation 3-6. This EOM indicates that the system behaves as a free vibration system. This assumes that the material mass is negligible such that once the mass drops on the material, the governing initial condition is the initial velocity of the mass. This assumption limits the model's ability to describe real impact scenarios where the effect of the material mass causes a transfer of momentum into the damping material.

$$m\ddot{x} + c\dot{x} + kx = 0 \quad (3-6)$$

By solving the differential equation with initial conditions of an impact velocity v_0 and zero initial displacement $x_0 = 0$, we obtain the displacement equation for the mass with time in Equation 3-7.

$$x = \frac{v_0}{\omega_d} e^{-\zeta \omega_n t} \sin(\omega_d t) \quad (3-7)$$

This is a standard second order model solution with $\omega_d = \omega_n \sqrt{1 - \zeta^2}$ and $\omega_n = \sqrt{\frac{k}{m}}$. From Table 3-1, the objective of this design problem is to minimize the acceleration of the dropping mass so Equation 3-7 is differentiated twice to obtain the acceleration expression given in Equation 3-8.

$$a = v_0 e^{-\zeta \omega_n t} \left(\frac{\zeta^2 \omega_n^2}{\omega_d} \sin(\omega_d t) - 2\zeta \omega_n \cos(\omega_d t) - \omega_d \sin(\omega_d t) \right) \quad (3-8)$$

The maximum acceleration occurs when the rate of change of acceleration with time is zero i.e. $a_{max} = a|_{\frac{da}{dt}=0}$. By evaluating the zero point of the acceleration derivative, the time at which the maximum acceleration is reached can be determined and used to obtain an expression for the maximum acceleration. Equation 3-9 is the time t_1 at which maximum acceleration is reached and by substituting it into Equation 3-8, we obtain Equation 3-10 which is the expression for the maximum acceleration in the system described by Figure 3-1.

$$t_1 = \frac{\tan^{-1} \left(\frac{\omega_d (3\zeta^2 \omega_n^2 - \omega_d^2)}{\zeta \omega_n (\zeta^2 \omega_n^2 - 3\omega_d^2)} \right)}{\omega_d} \text{ for } \zeta < 1 \quad (3-9)$$

$$t_1 = 0 \text{ for } \zeta \geq 1$$

In Equation 3-10, the damping ratio ζ and natural frequency ω_n are material dependent properties that must be substituted with the equivalent fundamental material parameters to complete the performance equation. Most viscoelastic damping materials, including the ones showcased in this study, exhibit a damping ratio of $\zeta < 1$. Hence, these materials are the focus of this study.

$$a_{max} = a(t = t_1) = v_0 \omega_n \frac{e^{\frac{\zeta \tan^{-1}\left(\frac{\sqrt{1-\zeta^2}(4\zeta^2-1)}{\zeta(4\zeta^2-3)}\right)}{\sqrt{1-\zeta^2}}}}{\zeta \sqrt{\frac{1}{\zeta^2(4\zeta^2-3)^2}(4\zeta^2-3)}} \quad (3-10)$$

For the system described in Figure 3-1, the natural frequency depends on the stiffness and the mass as $\omega_n = \sqrt{\frac{k}{m}}$. For congruency in material comparison, the dropping mass must remain the same as the stiffness varies depending on the material's molecular arrangements as explained in Chapter 2.2. The two viscoelastic material parameters introduced in Chapter 2.2 were storage modulus and loss factor so the next step is to define the equivalent stiffness and damping ratio in Equation 3-10 in terms of the storage modulus and loss factor.

3.1.1 Equivalent Stiffness and Damping Coefficient

The use of stiffness k and damping coefficient c used in deriving Equation 3-10 is to take advantage of known standard formulations to this design problem. While convenient, they are not readily available material data as described in Chapter 2.2. The Kelvin-Voigt model's similarity as explained in Chapter 3.2 is essential to finding the equivalent stiffness and damping in terms of storage modulus and loss factor.

The Kelvin-Voigt model behaviour under dynamic load represents a constant storage modulus which was not the observed case for the materials available. However, its similarity to the viscous model simplifies the analysis therefore its effect in the results will be discussed during validation. Figure 3-2 shows the second order viscous model with its parameters and the resulting Argand plane in Figure 3-3.

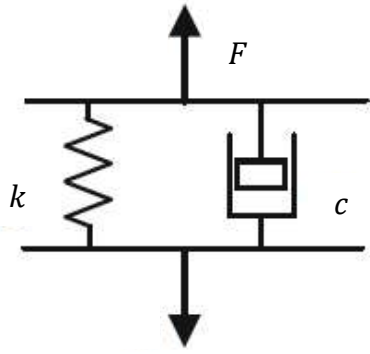


Figure 3-2: Viscous Model for Viscoelastic Materials

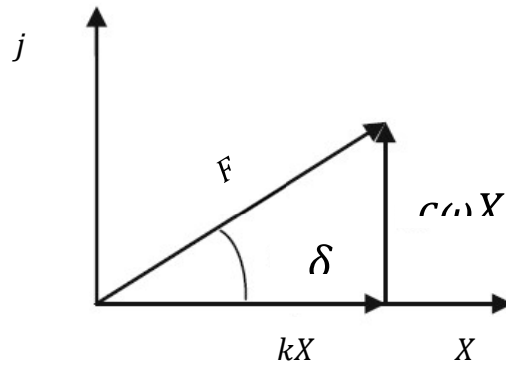


Figure 3-3: Argand Plane representation of Viscous Model

Figure 3-3 is the Argand plane describing the viscous model in phasor notation which is denoted by Equation 3-11. The transition to the complex domain using phasor notation incorporates frequency which is an important parameter in viscoelastic material behaviour.

$$\mathbf{F} = (c\mathbf{j}\omega + k)\mathbf{X} \quad (3-11)$$

The equivalent stiffness and damping coefficient k and c can be obtained directly from experimental results using the formulae from Figure 3-3. Equation 3-12 and Equation 3-13 are the equivalent stiffness and damping coefficient in terms of measurable experimental parameters.

$$k = \frac{|F|}{|X|} \cos \delta \quad (3-12)$$

$$c = \frac{k \tan \delta}{\omega} \quad (3-13)$$

The Stiffness k of a material under compressive load is also a product of the material area A and thickness L and its Modulus of elasticity given by Equation 3-14.

$$k = \frac{A}{L} E' \quad (3-14)$$

The material's modulus of elasticity determines the elastic response in viscoelastic materials and is defined as the storage modulus, E' , in Chapter 2.2. By substitution, the damping coefficient c is expressed in terms of measurable properties and the geometric parameters in Equation 3-15.

$$c = \frac{A}{L} \frac{1}{\omega} E' \tan \delta \quad (3-15)$$

Using the relationship between the loss and storage modulus from Chapter 2.2, Equation 3-15 is simplified to Equation 3-16.

$$c = \frac{A}{L} \frac{E''}{\omega} \quad (3-16)$$

3.1.2 Impact Model Ashby Performance Equation

With stiffness and damping coefficient defined in terms of viscoelastic material parameters, the equivalent damping ratio ζ can now be substituted into the performance equation for acceleration in Equation 3-10. The relationship between ζ and c is given by Equation 3-17 for a second order system.

$$\zeta = \frac{c}{2m} \frac{1}{\omega_n} \quad (3-17)$$

From Equation 3-16, we replace the damping coefficient c and obtain a damping ratio expression consisting of material parameters and geometric constraints in Equation 3-18.

$$\zeta = \frac{A E''}{L \omega} \frac{1}{2m\omega_n} \quad (3-18)$$

The two frequencies in Equation 3-18 represent the causing frequency ω and the system natural frequency ω_n . If the design purpose is to isolate higher frequencies, then the two frequencies differ and the simplified damping ratio ζ is given by Equation 3-19. Therefore, material selection is iterative because the behaviour changes with mass and geometry so the best performing material changes with each iteration. Moreover, the Ashby performance equation generated is not separable in to functional, geometric and material parameters as per the Ashby method.

$$\zeta = \frac{\sqrt{A}}{2\omega\sqrt{Lm}} \sqrt{E'} \tan \delta \quad (3-19)$$

When the two frequencies in Equation 3-18 are similar, that is the system is excited at its natural frequency and the damping ratio is simplified to Equation 3-20. The derivations for ζ are provided in Appendix B.1.

$$\zeta = \frac{\tan \delta}{2} \quad (3-20)$$

Equation 3-20 has been adopted in several literature [21]–[25] without discussion of its limitations in use but Carfagni et. al [26] discussed its shortcomings in application based on inherent non-linearity for viscoelastic materials. This definition is still adopted in education literature [21] and design conditions [24] so there is merit to it and this is particularly true for impact absorption. This is because when a material is subjected to a wide array of frequencies during an impact, the amplitude is attenuated at all frequencies but amplified at its natural frequency. Therefore, designing at or around the natural frequency is a good measure of a materials damping performance for impact absorption. In Chapter 4, the process of obtaining the material properties at the natural frequency is explained.

Finally the impact absorption Ashby equation can be formulated by substituting the natural frequency ω_n and damping ratio ζ into Equation 3-10. This implies that the analysis done hereinafter considers the material performance at the natural frequency and is effective for impact absorption viscoelastic material selection. Equation 3-21 is the final impact Ashby performance equation for selecting a material that minimizes the maximum acceleration developed. Notably, the functional, geometric and material parameters can be grouped together in the Ashby method fashion and the material index can be identified. This material index can be used to select the best material for a given set of materials as long as their performance at their natural frequencies is known.

$$a_{max}^2 = \frac{v_0^2 A}{m L} E' e^{-\frac{2 \tan \delta \arctan\left(\frac{\sqrt{4 - \tan^2 \delta} (\tan^2 \delta - 1)}{\tan \delta (\tan^2 \delta - 3)}\right)}{\sqrt{4 - \tan^2 \delta}}} \quad (3-21)$$

From Equation 3-21, the material index is isolated and given by Equation 3-22. By plotting equal-performance contours using this index, the best storage modulus and loss factor combination can be determined for a given design problem. Figure 3-4 is a plot of the performance contours using the material index in Equation 3-21. These contours indicate the material loss factor and storage modulus combinations at different natural frequencies.

$$\text{Material Index} = E'e \frac{2 \tan \delta \arctan \left(\frac{\sqrt{4 - \tan^2 \delta} (\tan^2 \delta - 1)}{\tan \delta (\tan^2 \delta - 3)} \right)}{\sqrt{4 - \tan^2 \delta}} \quad (3-22)$$

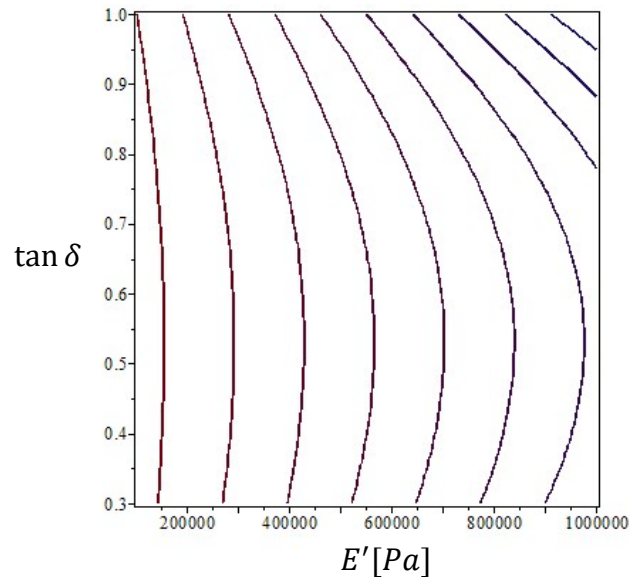


Figure 3-4: Impact Absorption Ashby Performance Curves

The aim of this analysis is to select a material that minimizes the maximum acceleration. Therefore, the lower the value of the material index in Equation 3-22, the lower the developed maximum acceleration on impact for a given material and mass with an initial velocity. In Figure 3-4, the better performing materials would be towards the bottom left corner of the plot. These contours show that a softer material is preferable since the better performing materials are towards the bottom left corner meaning that stiffness has a higher impact on performance than the loss factor. However, as materials get stiffer, the significance of the loss factor increases and the contour shape changes.

The different contours represent equal performance regions which means materials on the same curve perform equivalently. In other words, two materials on the same curve will result in the same acceleration based on the performance equation. After obtaining the material properties of loss and storage modulus through the procedure explained in Chapter 2.2.4.2, the designer plots them on Figure 3-4 and selects the better suited material based on its ranking. This significantly decreases the experimental work required in ranking material performance in different situations since the only required parameters are the material storage modulus and loss factor at the natural frequency.

However, engineering designers do not often have the luxury of extensively characterizing and modelling all materials before designing a product. Moreover, the contours in Figure 3-4 are obtained at the materials natural frequency which changes with changing geometric parameters of area and length in viscoelastic materials. This required complete re-characterization of material samples with each geometry change which is inefficient. Therefore, by creating design curves which incorporate all aspects of the design and require a single characterization improves selection of viscoelastic materials.

3.1.3 Impact Absorption Design Curves

Engineers often work with design curves when deciding what design options are suitable for the application. This is particularly true in construction industry where load bearing calculations are a common practice for pump or air conditioning unit selection. With design curves, an array of performance points is available instead of a single point as was the case with the Ashby performance curves in Chapter 3.1.2. Moreover, with a given set of design constraints, a designer can not only select the best performing option available but also know its performance based on the design point.

For impact absorption design, there are two cases considered in this study. In the first case, the designer wishes to minimize the acceleration of an object but does not know what material parameters are sufficient for the application. This is often the case for cargo planes and shipment vehicles where dropped items increase the wear and tear of the floor and potentially damage the items so the floor is cushioned by impact absorbing materials but the amount of material required is left to the discretion of the designer as long as the maximum acceleration developed on impact is minimized.

The second involves designing a for a given set of geometric and functional constraints. In cases where space limitations and performance specific conditions must be fulfilled, the designer is left to select the best performing material while meeting geometric and functional limits. One such design scenario is the selection of liner materials for helmets as discussed in Chapter 2.1.2. Helmets are designed for specific head mass, child or adult, and the amount of liner material is controlled by the helmet size as shown in Figure 2-1. The designer knows the mass of the intended user, as well as material geometric constraints of area and thickness and must select the best liner material that meets these limits while minimizing acceleration and determine what the maximum developed acceleration is to meet the HIC criteria.

In both design cases discussed above, Equation 3-21 is manipulated and used to generate design curves. By grouping impact velocity and developed acceleration, the geometric constraints and mass can be grouped to form their own design ratio and the material parameters form a third group. Equation 3-22 is the reformulated performance equation used to generate design curves. The acceleration and velocity are design parameters which can be grouped together while the area, thickness are material geometric parameters. The material properties can then be grouped together.

$$\left(\frac{a_{max}}{v_o}\right)^2 = \left(\frac{A}{Lm}\right) \left(E' e^{-\frac{2 \tan \delta \arctan\left(\frac{\sqrt{4-\tan \delta^2}(\tan \delta^2-1)}{\tan \delta(\tan \delta^2-3)}\right)}{\sqrt{4-\tan \delta^2}}} \right) \quad (3-23)$$

From Equation 3-23, we can generate material design curves with the performance, $\left(\frac{a_{max}}{v_o}\right)^2$, on the y-axis and the geometric and mass constraints, $\frac{A}{Lm}$ on the x-axis and the design curves are generated based on the material properties of storage modulus and loss factor from the rest of Equation 3-23.

Figure 3-5 shows an example of what such a graph would look like. The mass in each design point of the graph must be equal to the exact mass required to vibrate the system at its natural frequency. The experimental procedure as well as data manipulation to create the design curves in this study are covered in later chapters.

The two design cases introduced earlier are explained in Figure 3-5 by design arrows 1 and 2. For the first case, the designer begins with a desired maximum acceleration to velocity ratio and draws a horizontal line through all the materials and determines the corresponding $\frac{A}{Lm}$ ratio and decides which material is best suited for application based on the limiting criteria. It is important to note that the $\frac{A}{Lm}$ ratio is a maximum value limiting the combination of the material geometric parameters of area and length. By changing these values, one can lower the stiffness and improve the placement of the material in Figure 3-4. However, if area A and thickness L are fixed constraints, then the mass calculated is the critical mass at which the impact is amplified. Depending on the design curve shape, a higher or lower mass could improve or worsen the performance and this is to the discretion of the designer.

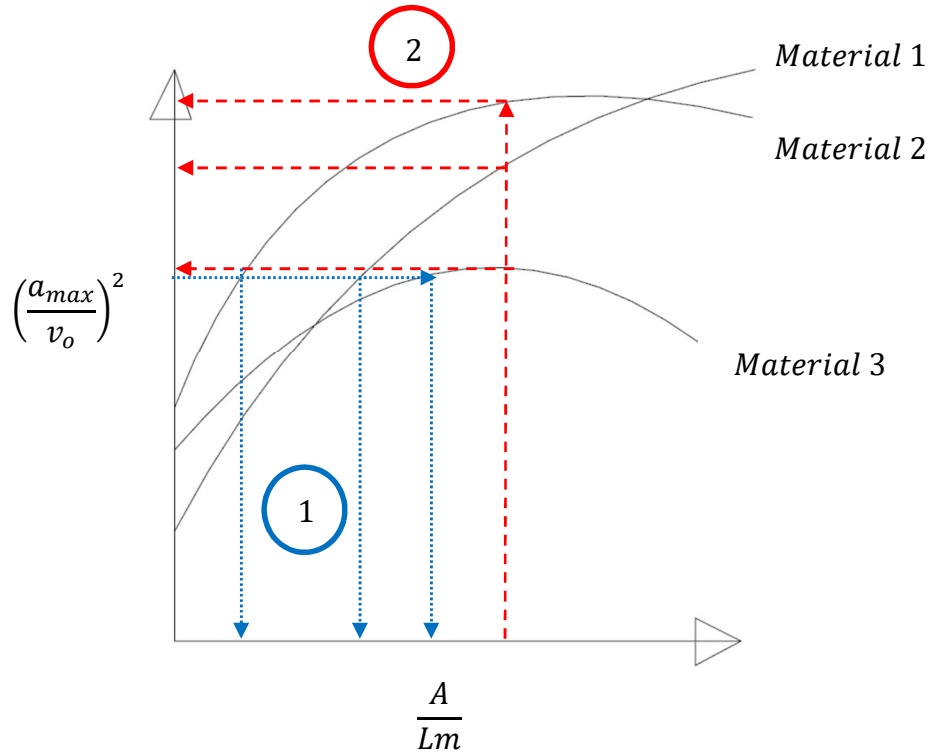


Figure 3-5: Sample Material Performance Design Curves

For case 2, the designer begins with a specific $\frac{A}{Lm}$ ratio and draws a vertical line through all the materials and determines the material performance ratio, $\left(\frac{a_{max}}{v_o}\right)^2$. For a given impact velocity, the lower the performance ratio the lower the developed maximum acceleration thus the better performing the material. For the example in Figure 3-5, Material 3 is the best choice for the given design point because it has the lowest performance ratio.

An important limitation not captured in these equations so far is the maximum achievable strain. Without limiting the maximum strain, a material can be compressed such that less energy is absorbed as it becomes compressed beyond its yield point. The maximum strain can be set based on performance standards and calculated based on the maximum acceleration from Equation 3-24. The derivations are presented in Appendix B.2. Once a material has been chosen, Equation 3-24 is used to verify the maximum strain achieved and verifies it against the set limits.

$$\epsilon_{max} = \frac{x}{L} = \frac{m \cdot a_{max}}{A \cdot E} \quad (3-24)$$

The purpose of Chapter 3 was to develop the concept of impact absorption by introducing the modeling. Using a viscous impact model and matching the material parameters with the Kelvin-Voigt model, the impact absorption performance equation was created. Using this equation, two design scenarios and their limitations were presented. Chapter 4 will review the instrumentation, experimental procedures, and data manipulation techniques. It will also present the design curves for the available materials. Chapter 5 then discusses the validation experiments conducted to verify the work presented here and discusses the implications as well as future avenues for further research in this field.

Chapter 4: Instrumentation and Data Analysis

Viscoelastic material behavior is affected by an array of parameters including frequency and degree of the load, temperature. A change in external conditions causes a shift in response as discussed in Chapter 2. Therefore, measuring the response of viscoelastic materials requires specialized equipment and a predetermined set of experimental parameters for consistent results. Moreover, the interpretation and use of viscoelastic material data in modelling must remain within the bounds of the experimental parameters in that extrapolation of data produces inaccurate information.

For the purposes of the analysis conducted in Chapter 3, two material parameters; the storage modulus E' and loss factor $\tan \delta$, were identified as the necessary variable in selecting the best performing materials for impact absorption. The selection techniques require these two properties over a range of frequencies to produce reliable design curves. Therefore, dynamic analysis of the available material samples is conducted within the linear viscoelastic range using a dynamic mechanical analyzer. This is further discussed in the subsections that follow.

4.1 Dynamic Mechanical Analysis & Linear Viscoelasticity

Viscoelastic dynamic properties are obtained in frequency controlled experiments observing and recording the material response to an input force. The deflection due to the applied force is measured as well as the phase difference between the force and deflection. The measured deflection is used to determine the strain on the material and the phase difference, δ determines the loss factor $\tan \delta$. In the present work, the instrument used to characterize the material behaviour over a range of frequencies is the Dynamic Mechanical Analyzer (DMA), specifically the DMA Q800 [27] shown in Figure 4-1.

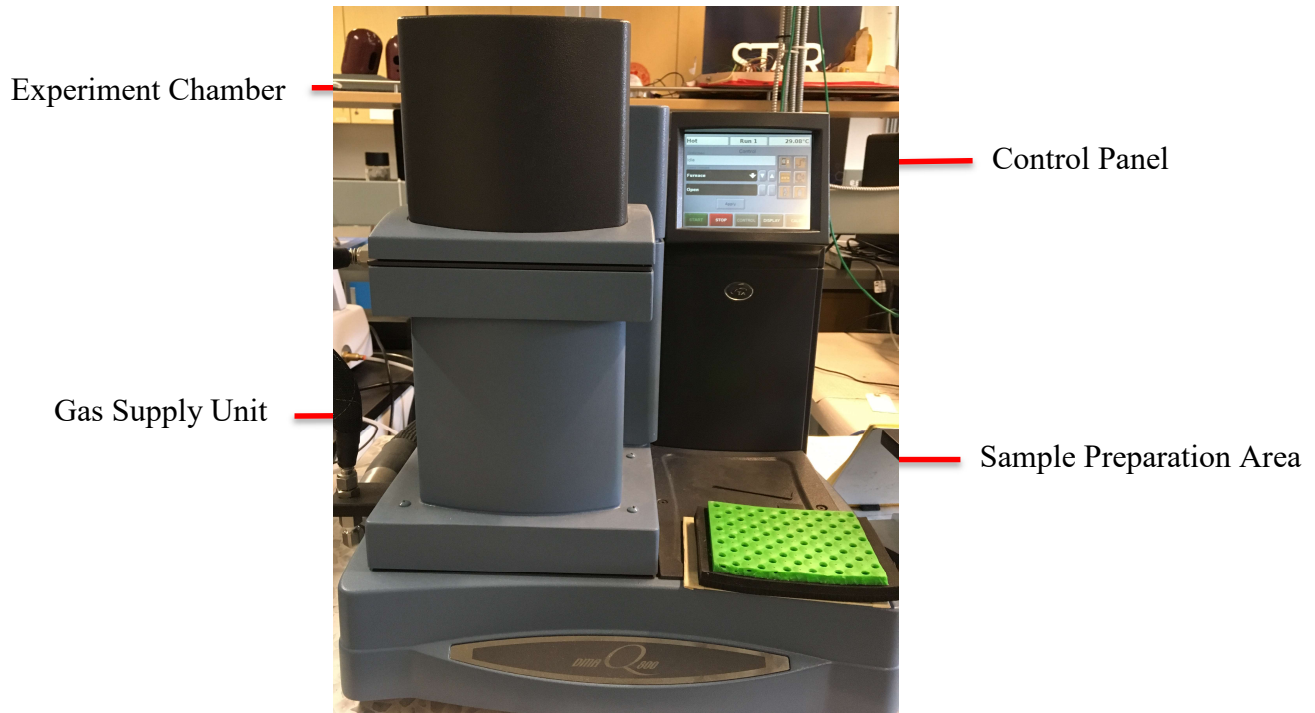


Figure 4-1: DMA Q800 (© Stephen Kimanzi)

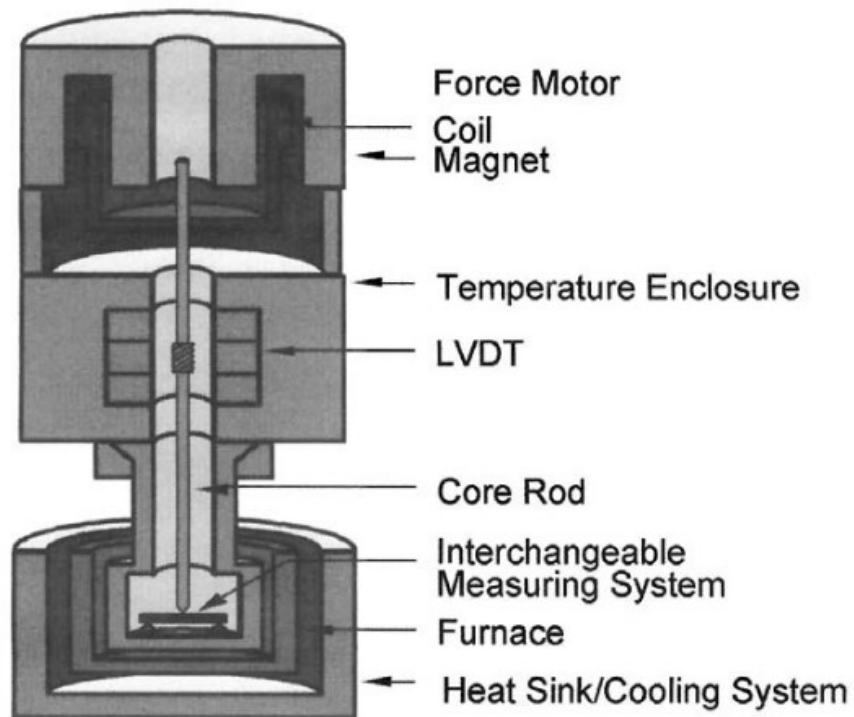


Figure 4-2: Typical DMA Configuration (© 1999 Kevin Menard, by permission)

In [28], Menard discusses the fundamental principles of DMA operation being the application of a force and measuring the deflection which is then used to infer the material behaviour. A typical DMA setup is shown in Figure 4-2 where the force motor and LVDT work to impart sinusoidal excitation on the sample and measure its response.

The oscillatory applied force produces a sinusoidal response as shown in Figure 4-3 and the dynamic force F_d is the applied oscillatory load while the static force F_s is the clamping force necessary to maintain the sample in position between the clamps and avoid contact loss during oscillation [28].

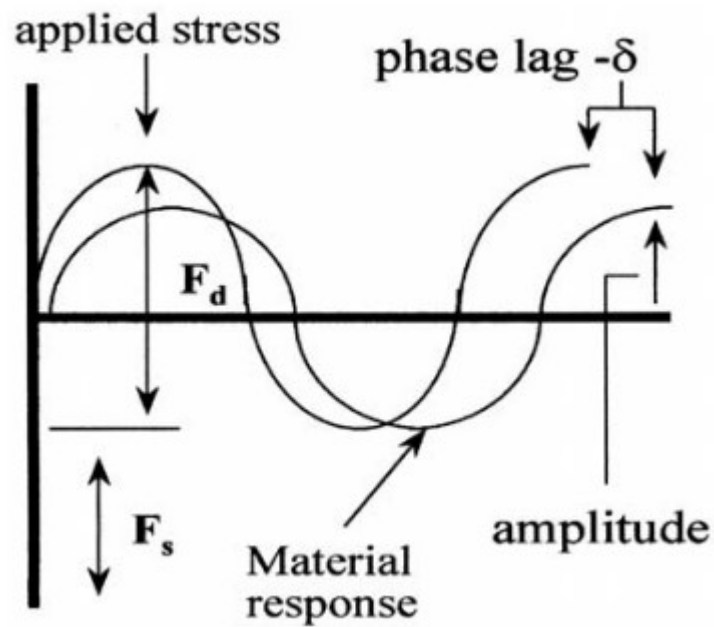


Figure 4-3: DMA Sinusoidal Force-Displacement Plot (© 1999 Kevin Menard, by permission)

The DMA design allows for variable frequencies in an experiment as well as studying the temperature response of materials. Moreover, there are multiple modes of deformation available for the designer including tension, compression, bending and shear for the Q800 [27]. More information on the intricate functionalities of the Q800 and the steps taken to characterize materials in this study are covered in Chapter 4.2.

An important consideration when determining the properties of viscoelastic materials is range through which the load deforms the material. Small and slow deformations ensure that the molecular arrangement is never far from equilibrium [27], [28] and the mechanical reflects the dynamic behaviour at the molecular level. This is called the Linear Viscoelastic Range (LVR) where the magnitudes of stress and strain are linearly related and a single function of time sufficiently describes the behaviour of any liquid [27], [28].

This consideration applies to all the viscoelastic models introduced in Chapter and in Figure 4-4, the LVR is identified in terms of the strain amplitude and the critical strain is identified to be the point at which the LVR ends and all the formulations for viscoelastic materials introduced in Chapter 2 do not hold. In [27], the LVR is defined to be 0.02% to 1% which is adhered to in the experimental work conducted in this analysis.

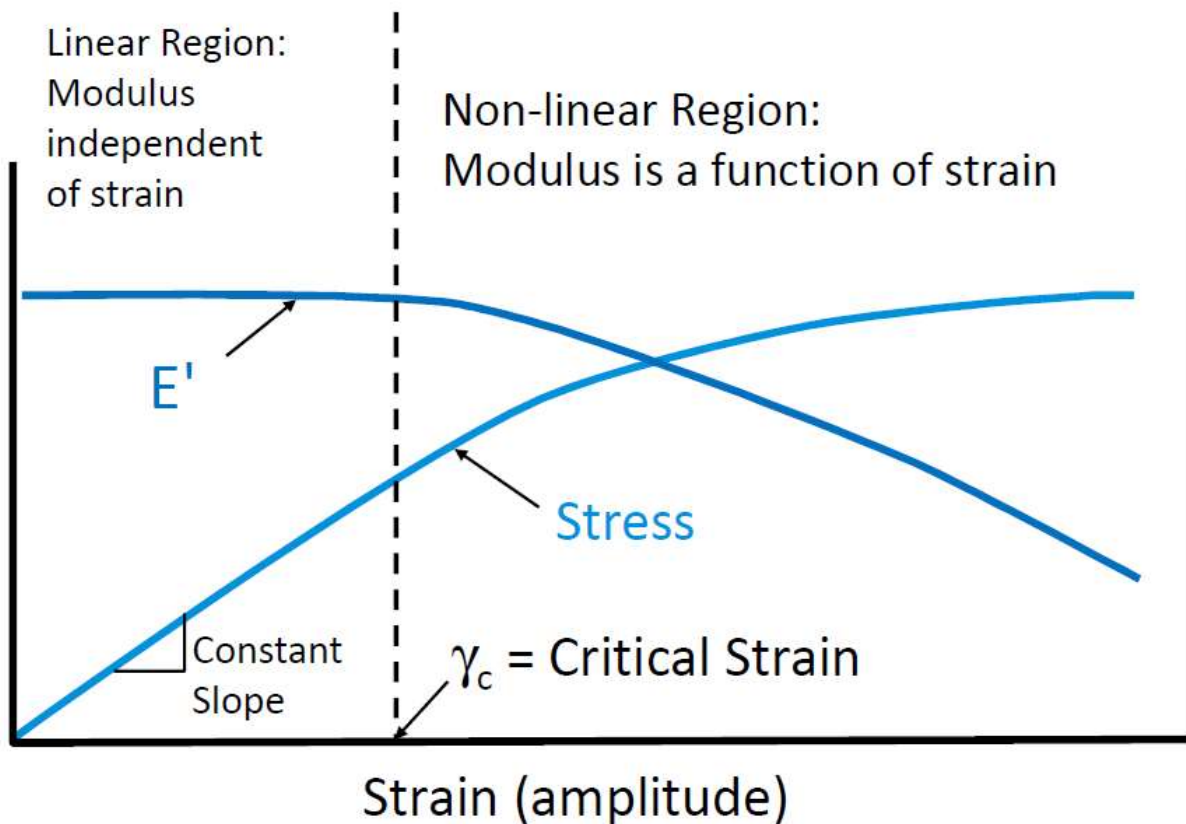


Figure 4-4: Linear Viscoelastic Range Behavior [36]

4.2 Experimental Procedure

Initially, the characteristics of the four materials available for analysis were unknown and their behavior as well their LVR. A frequency and strain sweep was conducted for each material sample to get an idea of their behavior as well as understand the saturation limits of the dynamic analyzer used. This Chapter covers the instrument used by discussing its calibration and limits, the material samples and the effect of sample size, and the instrument signal measurement and calculations.

4.2.1 DMA Q800

The DMA Q800 is a TATM instrument that includes a combined motor and transducer as shown in Figure 4-5 for the axial deformation mode. As the sample is deformed between the plates through the force applied by the motor, the displacement sensor determines the strain. There are several deformation modes available with the Q800 [27] and compression was used for this analysis.

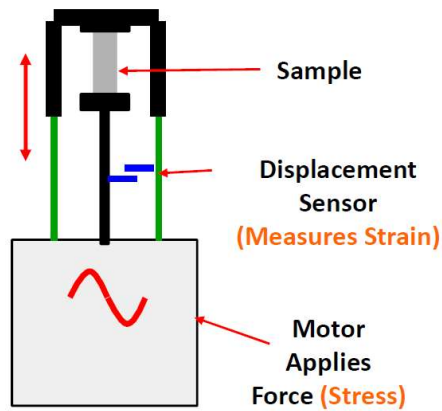


Figure 4-5: DMA Q800 Schematic for axial deformation mode [36]

Table 4-1 summarizes the Q800 specifications which identifies the instrument limits considered during the material characterization process.

Table 4-1: Q800 Specifications [36]

Max Force	Min Force	Frequency Range	Dynamic Deformation Range
18N	0.0001N	0.01 to 1250 rad/s 1.6e ⁻³ to 200 Hz	+/- 0.5 to 10,000 μm

With the DMA Q800 specifications determined, each material was subjected to a frequency scan from 10 Hz to 100 Hz and a strain sweep from 0.1% to 1%. The instrument was calibrated based on the steps outlined in [27] for the clamp mass, zeroing and compliance. There are two clamps available for the Q800, 15mm and 40mm diameter clamps. From the calibration results, the 15mm diameter clamp recorded a better compliance than the 40mm compliance. The influence of the material samples under compression on using the 15mm clamp over the 40mm is covered in Chapter 4.2.2.

The DMA was programmed for a frequency sweep from 10 Hz to 100 Hz under a constant temperature of 28 degrees Celsius under a constant deformation strain of 0.3% which is well within all the sample LVR. Moreover, this strain did not cause the DMA to exceed its maximum force which was a challenge encountered in the initial experiments. The offset force [27] was set to 0.1 N to ensure the sample did not detach during the cycles and a force track of 125% was used. The force track, as explained in [27], is a static force applied proportional to sample modulus since the behavior of viscoelastic materials is frequency variable and fixed static force alters the results.

The final material characterization data was collected by conducting three replicates for each material sample and the raw data and processing methods are covered in Section 4.3.

4.2.2 Material Samples

The compression clamp kit for the Q800 contains a sample coring tool that is capable of producing 12mm diameter samples. These samples are ideal for the 15mm clamp and cover majority of the clamp. For the 40mm clamp, 22mm square samples were used but the results were not scientifically sound. For a larger sample, the stiffness increases and so does the force for the same deflection. However, the results did not follow this logic and coupled with the compliance issues for the larger clamp identified in Chapter 4.2.1, the 15mm clamp was the choice for material characterization.

Table 4-2 summarizes the material sample dimensions. These samples were obtained from McMaster Carr in the U.S. and were observed to have no damage or defects on arrival.

Table 4-2: Experimental Sample Dimensions and Typical Specifications

Material	Thickness [mm]	Diameter [mm]	Typical E' (MPa)	Typical $\tan \delta$
Neoprene ² [29]	6.03	12.08	3.0 – 7.9	0.2 – 0.5
Rubber ³ [29]	5.92	12.70	3 – 8.1	0.03 – 0.1
Sorbothane ⁴ [30]	6.01	11.67	0.3 – 0.6	0.3 – 0.69
Santoprene ⁵	6.55	12.13	N/A	N/A

The experimental work and analysis assumes the samples to be perfect cylinders ignoring the effects of rough edges from the coring. The DMA measures raw signals of force and displacement and uses the material dimensions to generate properties like stiffness and storage modulus. The DMA signal processing is covered in Chapter 4.2.3.

4.2.3 DMA Instrument Calculations

The DMA measures the applied force, F_A , the resulting deformation amplitude, X_A and the phase difference, δ , between them. The measured stiffness k_s is calculated by $k_s = \frac{F_A}{X_A}$ and the DMA applies a pre-programmed geometry correction factor, $F_e = \frac{k_s}{k}$, to account for transverse strain [27], [31]. This correction factor applies to all materials and is introduced to account for the effect of

² Properties obtained at 10 Hz at room temperature

³ Properties obtained at 1 Hz

⁴ These values are taken at 10% strain with dynamic deformation ranging from 5 - 50 Hz

⁵ Unable to obtain dynamic compression data.

transverse strain during axial deformation [31]. An ideal axial deformation occurs vertically without any bulge effects i.e. transverse strain but this does not happen in practice which leads to a reduced measured stiffness. In order to account for the reduced measured stiffness, the instrument is programmed to generate a correction factor F_e which is based on the sample dimensions [31]. These values are based on an assumed Poisson ratio which quantifies the ratio of transverse to axial strain.

With the corrected material stiffness, the storage modulus E' is calculated using the sample area and thickness $E' = \frac{kL}{A}$ and the loss factor is directly calculated from the measured phase difference as $\tan \delta$. However, the DMA's calculated storage modulus does not consider the effect of the loss factor as explained in Chapter 2 when experimentally determining viscoelastic properties. This assumption is acceptable for low loss factor materials but the disparity is as high as 17% for high loss factor scenarios from experimental observations. Due to these inconsistencies, all material parameters will be calculated from the raw data using the Kelvin-Voigt model expression as discussed in Chapter 3. Chapter 4.3 covers data processing for impact absorption. The resulting material properties from this calculation compare well with the available literature data in Table 4-2 which further validates this method compared to directly using the produced DMA results.

4.3 Data Processing

The DMA's processed data was deemed inconsistent for this analysis in Chapter 4.2 but its raw signals can still be used to experimentally calculate the material parameters using the formulae in Chapter 2. The raw signals from the frequency sweep were the amplitude of the force, F_A , the deformation amplitude, X_A , and the loss factor, $\tan \delta$. The geometric parameters of area, A , thickness, L , and the resulting correction factor, F_e , were also used in generating material properties.

The true material stiffness k is calculated using the amplitude force and displacement as well as the correction factor given by Equation 4-1.

$$k = \left(\frac{F_A}{X_A} \right) / F_e \quad (4-1)$$

Using the true stiffness, the storage modulus E' is given by Equation 4-2.

$$E' = \frac{kL}{A} \cos \delta \quad (4-2)$$

The next step is to determine the mass required to convert the causing frequency to the system natural frequency. The calculation in Equation 4-3 assumes that material linearity is maintained for the calculated mass since the DMA raw signals are obtained within the LVR. This assumption admits numerous faults since it is highly likely that a higher mass would cause strains outside the LVR. For this reason, the validation experiments in Chapter 5 discuss the disparity between the DMA and measured material parameters.

$$m = \frac{k}{\omega_n^2} \quad (4-3)$$

The natural frequency ω_n in Equation 4-3 is obtained from the frequency sweep results between 10 Hz to 100 Hz. This converts the material properties obtained from the frequency sweep to material properties at different natural frequencies making it possible to generate design curves over a range of performance points. These performance points are given in terms of the $\frac{A}{Lm}$ ratio as explained in Chapter 4.2 and for each point, a corresponding maximum developed acceleration to initial velocity ratio $\left(\frac{a}{v_o} \right)^2$ is determined. Table 4-3 summarizes the material properties and how they are determined.

Sample raw material data tables are provided in Appendix C.1.

Table 4-3: Material Property Summary

f [Hz]	F_A [N]	X_A [μm]	$k = \frac{\left(\frac{F_A}{X_A}\right)}{F_e}$ [N/m]	$\tan \delta$	$E' = \frac{kL}{A} \cos \delta$	$m = \frac{k}{\omega_n^2}$	$\frac{A}{Lm}$
10
\vdots	\vdots	\vdots	\vdots	\vdots	\vdots	\vdots	\vdots
100

Data from each of the three replicates was processed and averaged to generate the final material performance behaviour. There was little variation in material behaviour such that averaging did not alter the final performance data. The design curves and ranking are discussed in Sections 4.4 and 4.5.

4.4 Ashby Performance Ranking

The data obtained from the DMA experiments can be used to select the best performing material based on the Ashby performance curves presented in Figure 3-4. All the material performance data has been superimposed in the Figure 4-6 based on the data in Appendix C.1 Table C-1 to C-4. Here, the better performing material is towards the left of the chart which is primarily Sorbothane with Neoprene a close second.

However, this chart does not describe how much material thickness or area is required or what mass is being protected. Therefore, while Sorbothane is the better performing material in Figure 4-6, the amount of material required to achieve the performance can not be readily determined. Moreover, this chart only represents a single design point and more any change to the design parameters would require creating a new chart. These limitations indicate that it is much more useful to generate design curves than can predict the performance and allow for size optimization.

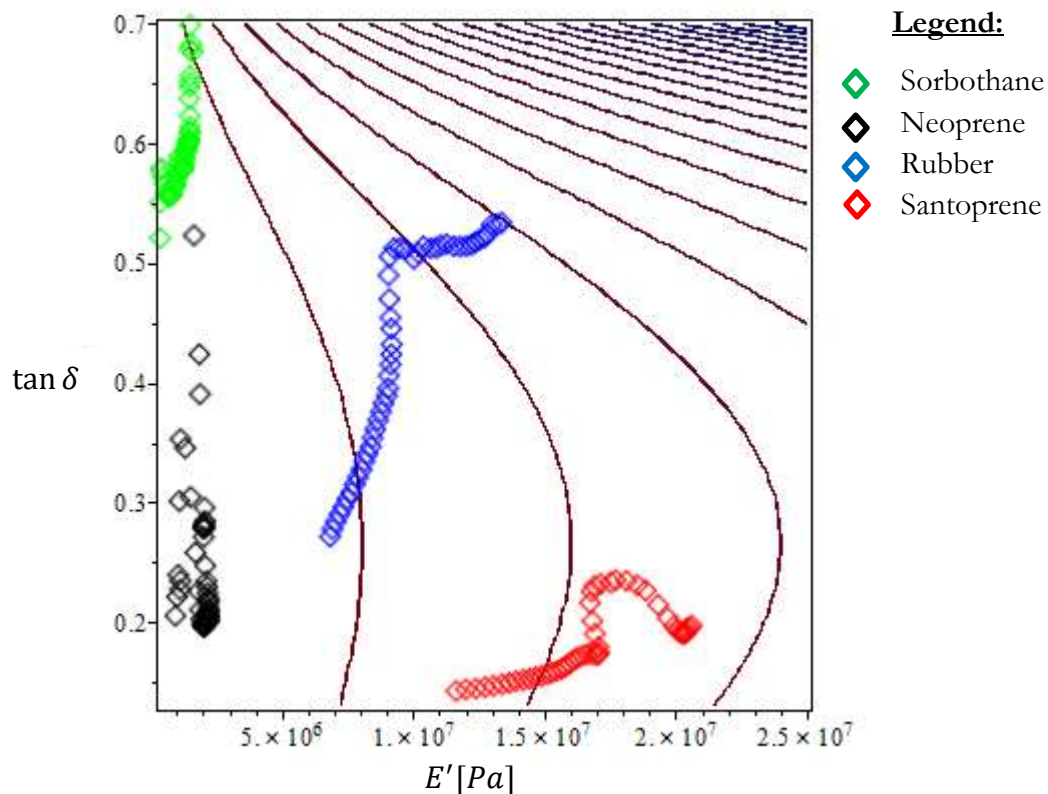


Figure 4-6: Superimposed Ashby Performance Curves for Material Selection

4.5 Design Curves and Material Ranking

The material performance over a wide range of design points was calculated based on the performance Equation 3-23 from Chapter 3. The performance $\left(\frac{a}{v_0}\right)^2$ is plotted against the design ratio of $\frac{A}{Lm}$ in Figure 4-7. The data for this graph is presented in Appendix C.1 Table C-1 to Table C-4.

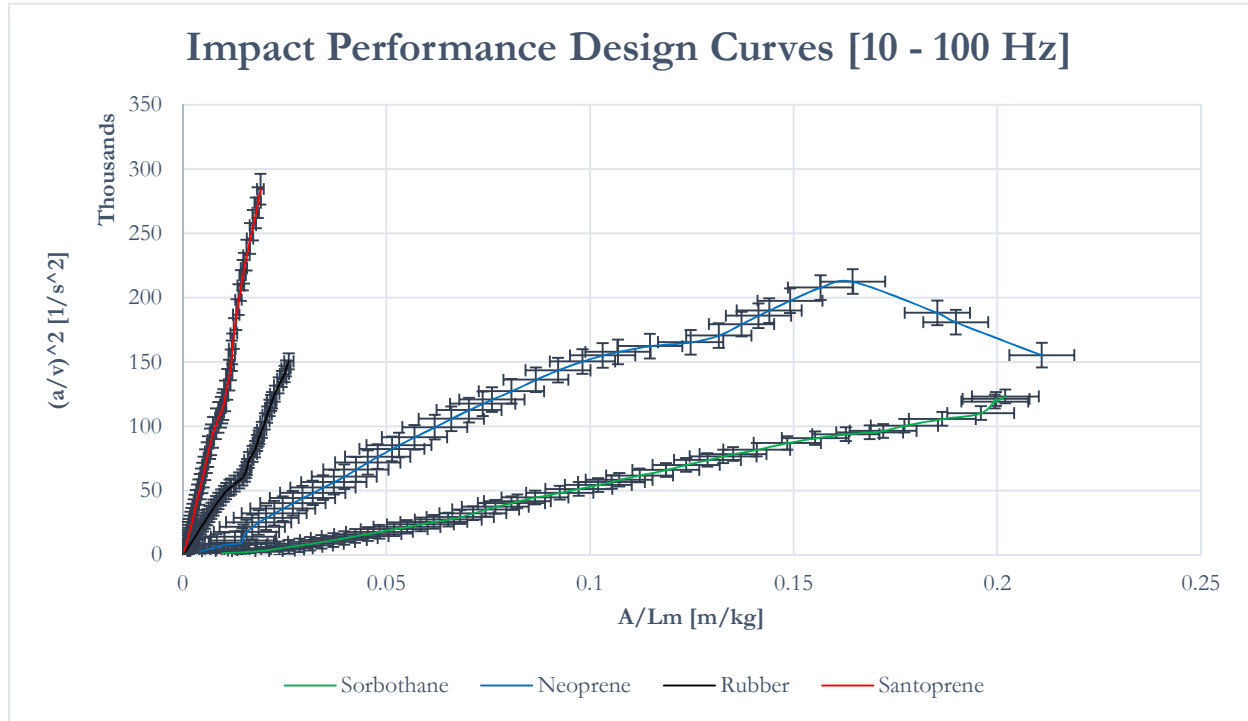


Figure 4-7: Material Impact Response Design Curves (with error bars)

The chart in Figure 4-7 is used by implementing the procedure in Chapter 3.2.3 by drawing a horizontal or vertical line depending on the design condition. If a designer has a target acceleration with a known starting velocity, a horizontal line is drawn to determine how much material is required for a given mass. Conversely, if a set amount of material is required to protect a given mass on impact, a vertical line determines the expected ratio of the developed maximum acceleration for an initial impact velocity.

On the x-axis, the $\frac{A}{Lm}$ ratio in $\frac{m}{kg}$ decreases towards the left as mass increases indicating that the maximum developed acceleration decreases with mass. This seems counterintuitive but it is logical since a heavier mass has a higher kinetic energy and thus displaces the material more such that it reaches zero velocity much later (zero velocity is the point of maximum acceleration⁶). A smaller mass has a lower kinetic energy and displaces the material much less hence achieves zero velocity much sooner developing a much higher acceleration in the process. This behaviour is observed for all materials except Neoprene which has a reversal around $\frac{A}{Lm} = 0.17 \frac{m}{kg}$. This is attributed to Neoprene's molecular composition which is outside the scope of this study but is worth reviewing in future work.

The y-axis shows the expected ratio of the maximum developed acceleration for an input velocity. The values are presented in Thousands for clarity which seems high at first but the actual maximum acceleration is obtained by determining the square root for a given input velocity. For instance, if an initial velocity of 1 m/s on a mass dropping on Neoprene at a design ration of approximately $\frac{A}{Lm} = 0.05 \frac{m}{kg}$, the expected maximum acceleration is 276 m/s^2 . This can be done for all materials at any ratio using any initial velocity.

⁶ The term acceleration here actually refers to the deceleration of the mass but the positive frame of reference is defined against gravity.

The data used in modeling and predicting the material behavior in Figure 4-7 is based on an average of 3 experimental runs. The added error bars represent the standard error in obtaining the expected acceleration using a given $\frac{A}{Lm}$ ratio or the expected standard error in calculating any of the three parameters in the $\frac{A}{Lm}$ ratio based on a known acceleration to velocity ratio. Majority of both the vertical and horizontal error bars overlap which shows that there is statistical insignificance between two close values. This could mean that the measurement resolution is not high enough to distinguish between two close performance points or that the material behavior does not drastically change between the two points. In Table 4-1, the DMA minimum force is 0.1 mN which is sufficiently high resolution but since the material stiffness is relatively high, very low deformation is imparted on the samples such that the differences in some of the produced data are statistically insignificant. This is observable in Figure 4-7 where the error bars for Rubber are much closer than those for Sorbothane and Neoprene since Rubber is much stiffer. Therefore, by conducting drop tower experiments, we can quantify the degree to which the margin of error impacts the prediction model's accuracy.

Finally, analysis of the four materials indicates that for the a given $\frac{A}{Lm}$ ratio, Sorbothane produces the least maximum acceleration followed by Neoprene, then Rubber, and then Santoprene. The validation experiments in Chapter 5 seek to confirm this order by observing the acceleration developed on impact using a drop tower setup.

Chapter 5: Validation and Discussion

The derivation of the material performance equation in Chapter 3 and material characterization techniques used to produce the design curves in Chapter 4 have made numerous assumptions which affect the reliability and accuracy of the results. By conducting impact absorption tests, the degree to which these assumptions impact the credibility of the design curves presented in Chapter 4 can be determined as well as the accuracy predicted acceleration ratios provided in Figure 4-7.

In Chapter 4, the material characterization data was obtained within the material LVR which is not representative of actual impacts where the produced strains are much higher and fall outside of the material LVR and the predicted response may deviate from that in Figure 4-7. This chapter discusses the drop tower experiments and compares the results to the predicted behavior in Chapter 4.

5.1 Validation Experiments

The impact experiments were conducted using an Instron CEAST 9340 fitted with an instrumented hemispherical impactor typically used for Compression After Impact (C.A.I) tests [32]. This system is calibrated to ASTM-D7136 standard which is used for measuring damage resistance of fiber-reinforced polymer matrix composites [33]. The hemispheric impactor is 16mm in diameter and is instrumented with a 4 MHz strain gauge sensor able to measure a maximum of 90 kN impact force. The mass of the impactor system is 0.837 kg with additional masses available for energy variation. Figure 5-1 shows the drop tower mechanism per the ASTM D7136 [33] design specification and the major components pertaining to the validation experiments.

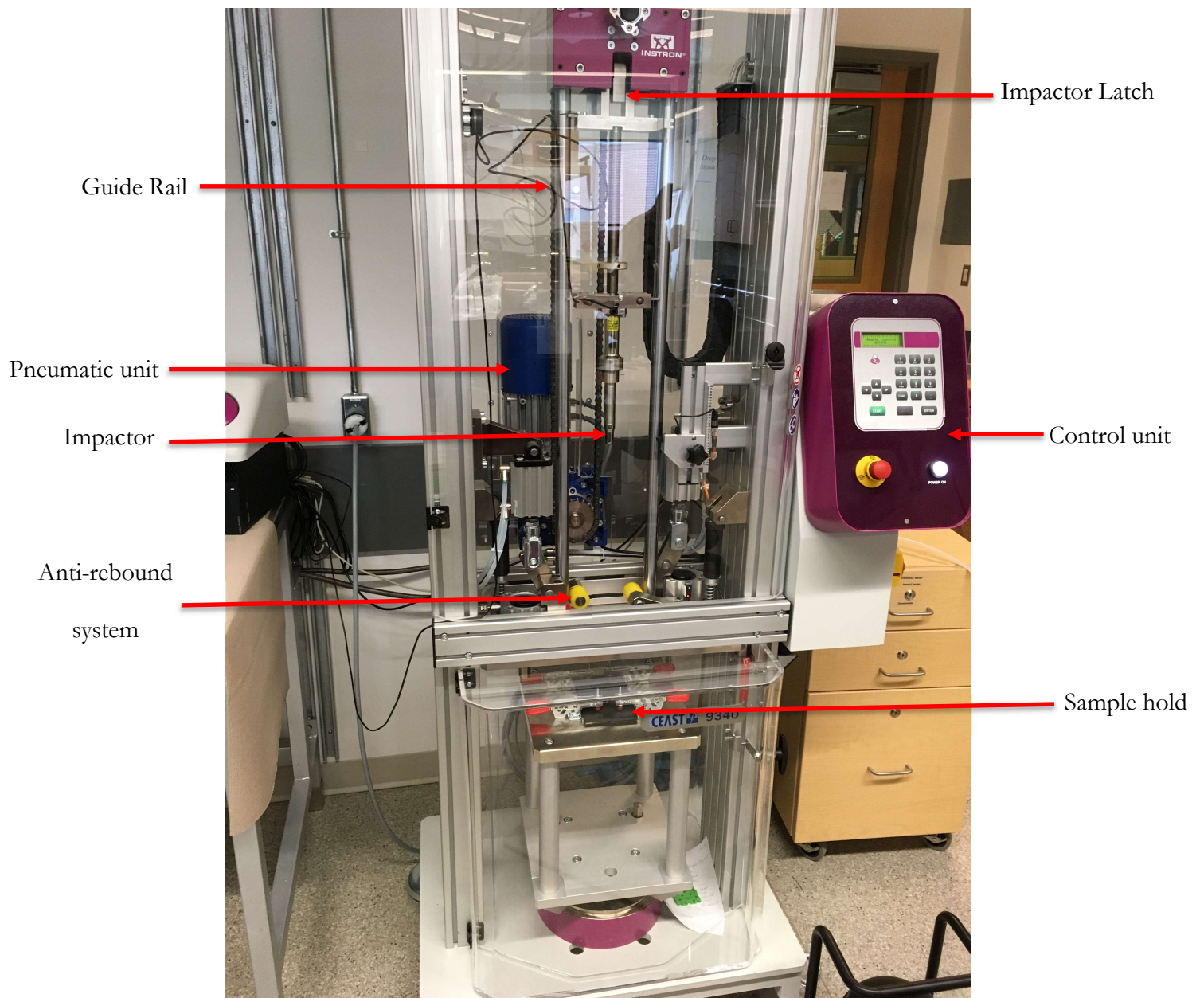


Figure 5-1: CEAST 9340 Drop Tower (© Stephen Kimanzi)

A 4 mm thick Steel plate is used to support the materials on the bottom as depicted in Figure 5-2. Using a steel plate is ideal since it is a stiff material and will not deform under impact thus will not absorb energy on impact and the recorded behavior is representative of the material response under impact. However, it is important to ensure that the material thickness is enough to avoid impacting the steel plate and recording higher impact forces.

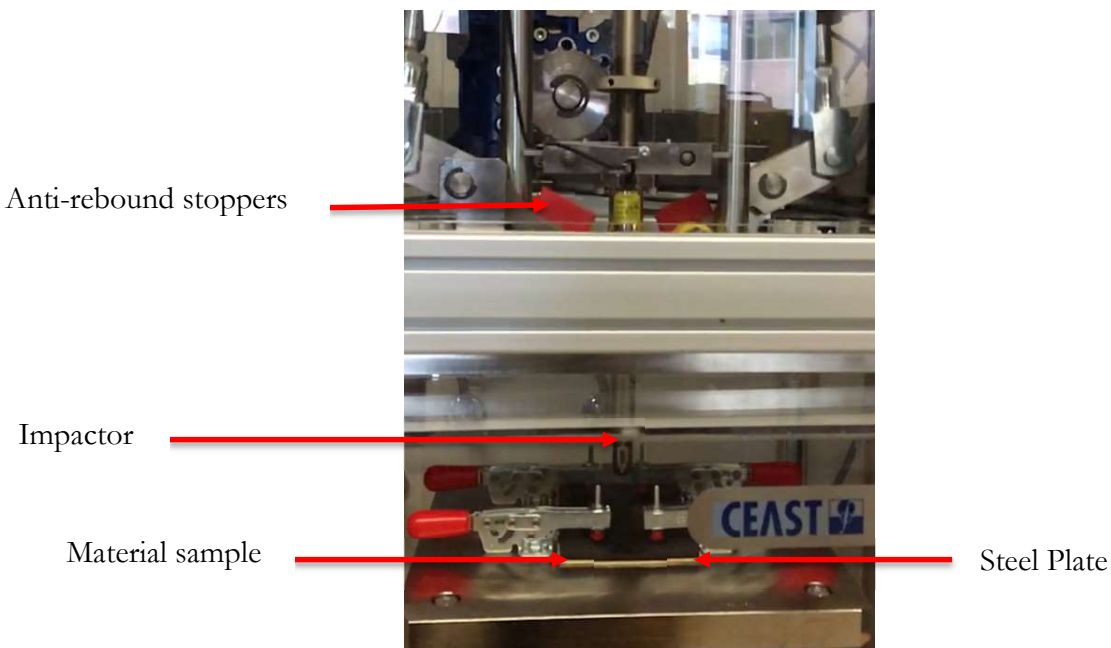


Figure 5-2: Supporting Steel Plate(© Stephen Kimanzi)

From the design curves in Figure 4-7, an initial design ratio of $\frac{A}{Lm} = 0.01$ was chosen as a design point of comparison based on the nominal material thickness (6.35 mm) and the effective area of the hemispheric impactor. The effective area is calculated from the circular impacted region defined by the diameter of the impactor. This is an approximation since the true area varies with each material as deformation changes but the intended use of the drop tower results as well as the shape of post impact deformation area on each material qualify the approximation.

The Instron CEAST 9340 is equipped with a photocell sensor that activates data collection at the point of impact and has an anti-rebound system that grabs the impactor after the initial impact [34]. This is useful in C.A.I tests because the fiber performance is studied for the initial impact but in this study, the anti-rebound system was switched off to study the amount of elastic energy stored in the material. An additional mass of 2.5 kg was introduced making the total impact mass 3.3370 kg. This was done to achieve the selected $\frac{A}{Lm}$ ratio. The impact velocity was 1 m/s to reduce the total amount of energy impacting the material which would significantly deviate from the LVR and make theoretical to experimental comparisons challenging. Moreover, 1 m/s velocity is easier to work with when calculating developed acceleration.

The sampling frequency was set to 500 kHz with a 40 kHz filter to reduce the noise from vibrations. Impact force is measured directly by the strain gauge sensors installed on the hemispheric impactor and using Equation 5-1, the developed acceleration is determined. As noted earlier, the positive frame of reference is defined against gravity which is subtracted from the developed acceleration.

$$a = \frac{F_{impact}}{m_{total}} - g \quad (5-1)$$

Figure 5-3 is a sample graph of the impact acceleration response with time from the first Sorbothane run. The shape of this graph resembles that obtained when simulating the second order model shown in Appendix B.3 although the positive frame of reference is reversed in the simulation. The high frequency at which data was collected is evident from the amount of noise on the graph.

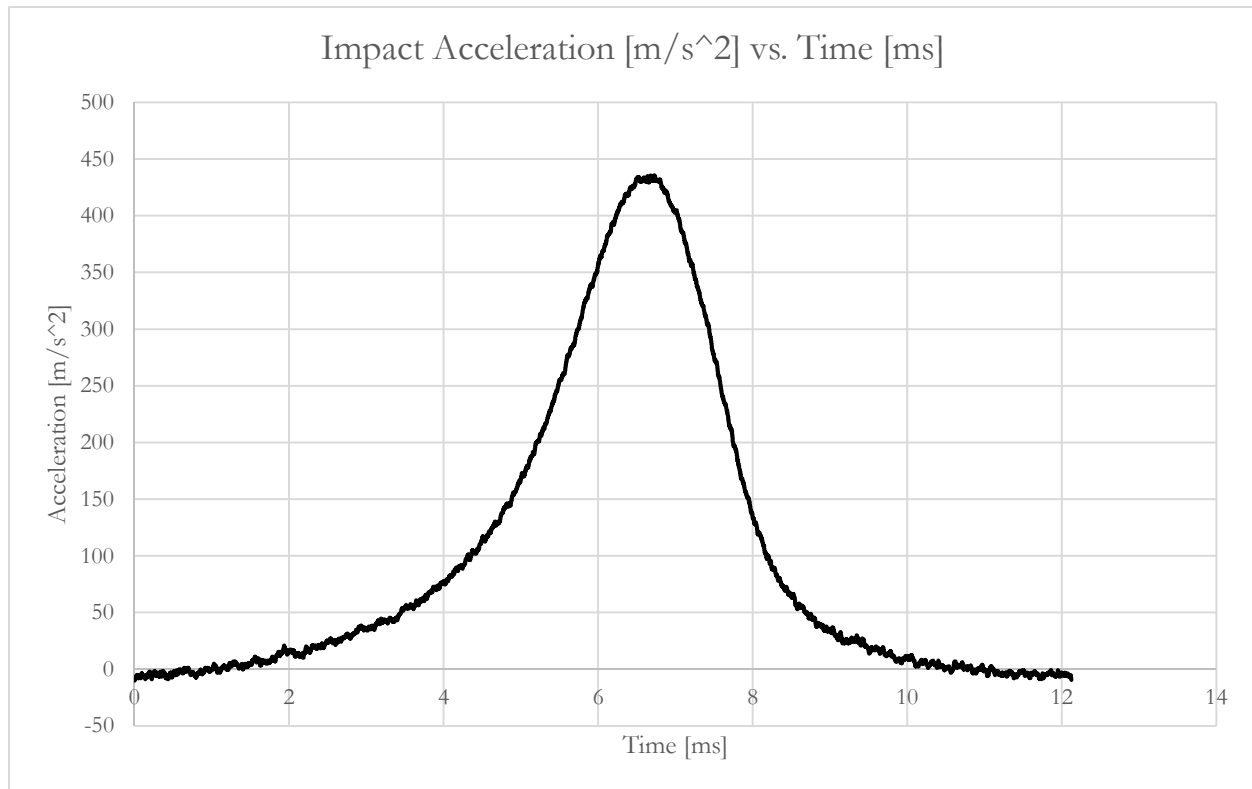


Figure 5-3: Sample Drop Tower Impact Response for Sorbothane

5.2 Discussion

The impactor delivered a total of 1.67 joules which generated high strains on the material samples such that the recorded maximum acceleration significantly differed from the predicted values from Figure 4-7 in Chapter 4. Table 5-1 summarizes the impact performance comparison for a single layer material. Sample calculations for the predicted peak accelerations are in Appendix C.2.

Table 5-1: Single Layer Material Performance, $\frac{A}{Lm} \cong 0.01$

Material	Predicted Peak Acceleration [m/s ²]	Measured Peak Acceleration [m/s ²]	Measured to Predicted Ratio	Peak % Strain	
				Predicted	Measured
Sorbothane	$\mu=51.40$ $\sigma=0.374$	$\mu=450$ $\sigma=10.761$	8.75	212.46	$\mu=88.40$ $\sigma=5.556$
Neoprene	$\mu=83.84$ $\sigma=2.477$	$\mu=363$ $\sigma=22.088$	4.33	148.71	$\mu=75.77$ $\sigma=2.881$
Rubber	$\mu=246.33$ $\sigma=0.815$	$\mu=310$ $\sigma=12.718$	1.26	45.92	$\mu=58.30$ $\sigma=2.131$
Santoprene	$\mu=330$ $\sigma=2.095$	$\mu=304$ $\sigma=10.504$	0.92	32.43	$\mu=67.86$ $\sigma=1.717$

For a performance ratio of $\frac{A}{Lm} = 0.01$, Figure 4-7 in Chapter 4 ranks the materials in descending order as Sorbothane, Neoprene, Rubber, and Santoprene. In Table 5-1, the measured acceleration values indicate the material performance is in reverse order with Sorbothane being the worst performer. This is due to the high strains required to produce such low accelerations which are physically impossible to achieve in compression since they would lead to a negative stiffness. For Neoprene and Sorbothane, the predicted strain is more than 100% in order to achieve the predicted acceleration but such a scenario cannot be attained. This also reflected in the predicted to measured ratio for acceleration

which is too high for Sorbothane and Neoprene while it is almost 1 for Rubber. We can note that for any feasible comparisons between the predicted and measured value to be made, the predicted and measured strains must be low and achievable i.e. closer to the LVR described in Chapter 4. Notably, the standard deviation for measured values are much higher than those for the predicted value. This is because the predicted values are based on low experimental noise measurements with little material deformation whereas the measured quantities were obtained from high experimental noise measurements where the material samples were deformed

With the knowledge that these inconsistencies are primarily due to the high strains developed during the drop tower experiments, it is necessary to increase the material thickness in the drop tower experiments. For this study, the available maximum material thickness is 6.35 mm. Therefore, multiple material layers are stacked together to increase the thickness which decreases the achievable peak strain. However, the thickness of the stacked material samples was limited to the maximum available sample space such that only a maximum of 3 layers was possible. This was compounded by the fact that the drop height was set at its lowest point to reduce the energy delivered on impact, the material layers could not be stacked to more than 3 layers to ensure the minimum distance between the sample and impactor was maintained.

In Table 5-2, the drop tower performance for two material layers is summarized. For this design point, the $\frac{A}{Lm}$ ratio is 0.005 because the thickness is doubled from the previous design point but the impact mass and area are constant.

Table 5-2: Two Layer Performance, $\frac{A}{Lm} \cong 0.005$

Material	Predicted Peak Acceleration [m/s ²]	Measured Peak Acceleration [m/s ²]	Measured to Predicted Ratio	Peak % Strain	
				Predicted	Measured
Sorbothane	$\mu=36.35$ $\sigma=0.177$	$\mu=158.25$ $\sigma=4.902$	4.35	151.03	$\mu=82.90$ $\sigma=1.723$
Neoprene	$\mu=55.58$ $\sigma=0.112$	$\mu=168.05$ $\sigma=0.700$	3.02	114.26	$\mu=61.29$ $\sigma=1.532$
Rubber	$\mu=169.51$ $\sigma=0.831$	$\mu=199.33$ $\sigma=17.175$	1.18	34.45	$\mu=39.58$ $\sigma=7.130$
Santoprene	$\mu=254.00$ $\sigma=2.943$	$\mu=178.56$ $\sigma=11.760$	0.70	49.6	$\mu=27.16$ $\sigma=0.825$

The addition of a second material layer decreases the peak strain achieved during impact and brings the ratio of predicted to measured accelerations much closer. There is also less spread in the data which is evident from the decrease in both the predicted and measured standard deviations for all material samples. This increases the data significance and further supports the proposition that lower predicted and measured strains lead to better matching between the predicted and measured accelerations and increases model validity. Moreover, the performance ranking from the predicted data closely resembles that of the measured data with Rubber and Santoprene switching performance ranking. Santoprene produces a lower peak acceleration than predicted which is attributable to a number of reasons summarized below:

- I. Santoprene is a Thermoplastic Elastomer (TPE) whose behavior is best modeled using the Maxwell-Wiechert model. The predicted results use a Kelvin-Voigt model for viscoelastic materials which could explain the disparity.

- II. Santoprene is not Anelastic i.e. it does not recover its shape once deformed and since the experimental data was obtained by averaging 3 replicates for the same material sample, the performance of Santoprene does not represent actual material behavior.

For Sorbothane, Neoprene, and Rubber, the measured value is approaching the predicted acceleration especially with a reduced peak strain. This is particularly true for Rubber which is now at ratio of 1.1.8 predicted to measured acceleration. It follows that if we achieve a lower experimental strain i.e. on that is closer to the LVR, the better the match is between the predicted and measured acceleration. However, once again the results for Rubber do not follow the trend of higher accelerations matching lower strains. For this performance point, the deviation in the peak measured strain for the Rubber runs was 7.1 which would explain the deviation from this trend.

Moreover, the drop tower runs that produced accelerations much similar to the predicted value were seen to follow the trend of higher accelerations corresponding to lower strains. Therefore, the averaging of the multiple runs impacts the matching of the data. The final drop tower validation experiments were conducted using 3 material layers to further decrease the peak strain and bring the predicted and measured values much closer.

In Table 5-3, the performance of 3 material layers is presented with the omission of Santoprene based on the reasons stated above. The aim of conducting the drop tower experiments with three material layers⁷ is to test the theory that the closer the peak strain is to the LVR, the closer the measured acceleration is to the predicted one in Chapter 4 Figure 4-5.

⁷ Three material layers were the maximum attainable level due to instrument sample thickness limitations and a higher overall sample curvature.

Table 5-3: Three Layer Performance, $\frac{A}{Lm} \cong 0.0033$




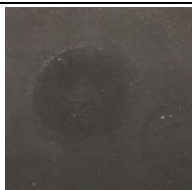




Material	Predicted Peak Acceleration [m/s ²]	Measured Peak Acceleration [m/s ²]	Measured to Predicted Ratio	Peak % Strain	
				Predicted	Measured
Sorbothane	$\mu=29.59$ $\sigma=0.09$	$\mu=73.99$ $\sigma=1.070$	2.50	123.63	$\mu=66.49$ $\sigma=N/A$
Neoprene	$\mu=46.46$ $\sigma=0.098$	$\mu=112.74$ $\sigma=1.400$	2.42	95.19	$\mu=28.20$ $\sigma=0.42$
Rubber	$\mu=135.65$ $\sigma=0.551$	$\mu=138.82$ $\sigma=6.402$	1.02	29.12	$\mu=20.15$ $\sigma=0.139$

The peak strains achieved with three material layers are much lower compared to those achieved using two material layers and a single material layer. Moreover, the predicted-to-measured ratios are getting closer to 1 with Rubber being the closest to its predicted value and the strains observed here follow the higher acceleration corresponding to lower strains. The standard deviation for peak strain for the Rubber runs in this case is 0.14. It is clearly evident that a lower peak strain produces a peak acceleration much similar to the predicted value in Chapter 4 Figure 4-7. This means that deforming the materials closer to their LVR results in a behavior that can be predicted based on low strain dynamic tests such as those conducted in Chapter 4 using a DMA at much lower strains. Notably, the predicted strain is consistently higher than the measured strain which is due to the linearity of the model used in predicting the material behavior. However, as more layers are added, the predicted and measured strains become increasingly similar which presents an opportunity to identify the limits of the prediction model.

It is evident that the selection model presented in this work is limited in its ability to predict materials whose viscoelastic behavior does not conform to that represented by the Kelvin-Voigt model as was the case with Santoprene. This implies that the designer must understand the behavior of the materials available for selection before embarking on a using the technique presented here to generate a design chart similar to the one provided in Figure 4-7. Moving forward, the modeling algorithm provided must be expanded to include a constraint for maximum achievable strain since it is physically impossible to achieve strains greater than 100% in compression. This constraint can be based on available design standards and should be accompanied by a lower mass and a reduced initial velocity in the drop tower experiments to ensure lower strains are developed in the material, especially for Sorbothane and Neoprene which are much softer than Rubber.

It is important to note here that except for Santoprene, the different runs of the drop tower experiments were conducted on the same material samples unless they got damaged during the experiment. The Santoprene sample had to be exchanged for every run since it is not anelastic. In Table 5-4, the before and after images and thicknesses are presented. The region of impact is visible in the “after” images and for Santoprene, it is clear that a deformation has occurred. The thickness measurements before and after show that Santoprene is the only anelastic material. This distinction is important because if the materials are not Anelastic, repeated impacts would not represent true material behavior. The samples shown in the images are from the 3 layer experiments since the single layer experiments recorded extremely high strains and some of the samples were damaged.

Table 5-4: Anelastic Material Behavior

Material Sample	Before Impact, T_1		After Impact, T_2	
Sorbothane $T_1 = 6.01mm, T_2 = 5.99mm$				
Neoprene $T_1 = 6.03mm, T_2 = 6.02mm$				
Rubber $T_1 = 5.92mm, T_2 = 5.92mm$				
Santoprene $T_1 = 6.55mm, T_2 = 6.42mm$				

Finally, it is unlikely that a complete agreement between predicted and measured data will be achieved due to the assumptions made in analysis including using a Kelvin-Voigt model to generate an equivalent behavior of the viscous model damping and stiffness elements. These assumptions limit the degree to which the predicted and measured values can match but the material ranking, which is the main aim of this analysis, is congruent when looking at the predicted and measured values and thus provides a basis for initial selection and trend observation before further characterization.

Chapter 6: Conclusion

The aim of this study was to devise a material selection process for viscoelastic materials to be used in impact absorption. The challenge with viscoelastic material selection, as discussed in Chapters 1 and 2, is the dependence of their material behavior to multiple parameters such as temperature and frequency. In this study, the influence of temperature was assumed negligible and all experimental work was conducted at a constant temperature leaving frequency as the main variable.

An impact model was developed using the viscous model and the Kelvin-Voigt model was used to relate the impact model to fundamental viscoelastic material parameters namely storage modulus E' and loss factor $\tan \delta$. The material performance factor for impact absorption was determined to be acceleration and the performance equation in Chapter 3 Equation 3-21 was generated by solving the second order equation of motion and isolating the point of maximum acceleration and substituting the equivalent viscoelastic material parameters based on the correlation between the viscous model and the Kelvin-Voigt model. Using a dynamic mechanical analyzer, the material properties at different frequencies were obtained and transformed to the properties at the various material natural frequencies based on the equivalent mass. This work produced design curves plotted in Figure 4-7 which can be used to predict the performance of a given material based on a given design ratio of geometric parameters and mass, $\frac{A}{Lm}$ and the impact velocity v_o .

The assumptions made in generating the performance equation and the subsequent design curves necessitated required validation experiments to quantify the degree to which the methods used impacted the accuracy of the produced results. A CEAST 9340 drop tower was used to deliver energy to various material configurations. The general performance ranked the materials with Sorbothane first, Neoprene second, and Rubber third. Santoprene was found to produce a lower acceleration than predicted which was attributed to the incompatibility of the modeling technique with Santoprene behavior. Moreover, a positive correlation was found between the peak strain developed during impact and the ratio of predicted to measured acceleration values, i.e. the closer the strain is to the LVR, the more accurate the predicted peak acceleration is to the measured value.

This research provides a simple starting point for viscoelastic material selection and design by bridging the gap between material behavior and complex modeling. By using simplified modelling techniques and providing experimental results, it shows that initial decisions on the impact performance of viscoelastic materials does not need complex modeling techniques or extensive experimental work.

There is still a need to explore the effect of using a different viscoelastic model such as the Maxwell-Wiechert model and compare the quality of data with that from using a Kelvin-Voigt model. Moreover, due to the observed effect of the peak strain, it may be necessary to set a limit on the achievable peak strain to limit the amount of material that can be realistically used to achieve the prescribed peak strain. Using the process of impact modeling and correlating the material parameters to the impact model presented here, differently behaving materials can also be studied. Finally, selecting a baseline viscoelastic material for impact absorption can be done without extensive characterization or experimental work and further detailed modeling and analysis is only necessary once the best performing material selected by using the techniques provided here.

Bibliography

- [1] R. Lakes, *Viscoelastic Properties of Materials*. 2017.
- [2] R. S. Lakes, *Viscoelastic Solids*. New York: Taylor & Francis, 1999.
- [3] R. S. Lakes, “Viscoelastic Solids,” p. 496, 1998.
- [4] R. Eksbergian, “Fundamentals of vibration analysis,” *J. Franklin Inst.*, vol. 262, no. 3, p. 233, 1956.
- [5] W. A. Siswanto, M. N. Ibrahim, M. A. Madlan, and S. M. Mohamad, “Shaker Table Design for Electronic Device Vibration Test System,” *Int. J. Eng. Technol.*, vol. 3, no. 6, pp. 663–668, 2011.
- [6] W. W. D. Askeland, P. Fulay, *The Science and Engineering of Sport Surfaces*. .
- [7] S. J. Dixon and V. H. Stiles, “Impact absorption of tennis shoe – surface combinations,” *Sport. Eng.*, vol. 6, pp. 1–10, 2003.
- [8] S. L. James, B. T. Bates, D. Ph, R. Louis, and D. Ph, “Injuries to runners,” no. 1.
- [9] A. T. A. Connor *et al.*, “Current Standards for Sports and Automotive Helmets : A Review,” pp. 1–42, 2016.
- [10] A. A. Sabet, E. Christoforou, B. Zatlin, G. M. Genin, and P. V. Bayly, “Deformation of the human brain induced by mild angular head acceleration,” *J. Biomech.*, vol. 41, no. 2, pp. 307–315, 2008.

- [11] S. Li *et al.*, “Temporal profiles of axonal injury following impact acceleration traumatic brain injury in rats-a comparative study with diffusion tensor imaging and morphological analysis,” *Int. J. Legal Med.*, vol. 127, no. 1, pp. 159–167, 2013.
- [12] C.-Y. Chang, C.-S. Ho, and S.-Y. Chang, “Design of a helmet,” pp. 1–43, 2003.
- [13] J. G. B. Derraik, H. Sciences, and N. Zealand, “The pollution of the marine environment by plastic debris: a review,” *Mar. Pollut. Bull.*, vol. 44, no. 9, pp. 842–52, 2002.
- [14] A. Grover, A. Gupta, S. Chandra, A. Kumari, and S. M. P. Khurana, “Polythene and environment,” *Int. J. Environ. Sci.*, vol. 5, no. 6, pp. 1091–1105, 2015.
- [15] M. F. Ashby, “Materials Selection in Mechanical Design (Fourth Edition),” 2011.
- [16] P. Sirisalee, M. F. Ashby, G. T. Parks, and P. J. Clarkson, “Multi-Criteria Material Selection in Engineering Design,” *Adv. Eng. Mater.*, vol. 6, no. 12, pp. 84–92, 2004.
- [17] A. J. Parker, “Cushioning Materials,” *Mech. Eng.*, no. May, 2007.
- [18] R. G. Larson, S. Goyal, and C. Aloisio, “A predictive model for impact response of viscoelastic polymers in drop tests,” *Rheol. Acta*, vol. 35, no. 3, pp. 252–264, 1996.
- [19] I. I. Argatov, “Mathematical modeling of linear viscoelastic impact: Application to drop impact testing of articular cartilage,” *Tribol. Int.*, vol. 63, pp. 213–225, 2013.
- [20] X. Q. Zhou, D. Y. Yu, X. Y. Shao, S. Q. Zhang, and S. Wang, “Research and applications of viscoelastic vibration damping materials: A review,” *Compos. Struct.*, vol. 136, pp. 460–480, 2016.

- [21] M. Brennan, "Vibration Control by Damping."
- [22] P. Macioce, "Viscoelastic Damping," *Sound Vib.*, pp. 4–5, 2003.
- [23] M. L. Lai, P. Lu, D. A. Lunsford, K. Kasai, and K. C. Chang, "Viscoelastic damper: A damper with linear and nonlinear material?," *11th World Conference on Earthquake Engineering*. pp. 1–8, 1996.
- [24] E. I. Rivin, "Materials Design : Vibration Isolation and Damping , the Basics," pp. 1–7, 2003.
- [25] E. E. Ungar and E. M. J. Kerwin, "Loss Factors of Viscoelastic Systems in Terms of Energy Concepts," *J. Acoust. Soc. Am.*, vol. 34, no. 7, pp. 954–957, 1962.
- [26] M. Carfagni, E. Lenzi, and M. Pierini, "The loss factor as a measure of mechanical damping," *SPIE Proc. Ser.*, pp. 580–84, 1998.
- [27] TA Instruments, "Dynamic mechanical analysis, basic Theory & Applications Training," *Encycl. Polym. Sci. Technol.*, vol. 9, pp. 563–590, 2004.
- [28] K. P. Menard and K. Peter, *DYNAMIC MECHANICAL ANALYSIS A Practical Introduction* .
- [29] W. M. Madigosky, "Dynamic Viscoelastic Properties of Selected Natural-Neoprene Rubber Blends," 1990.
- [30] S. Inc., "DATA SHEET 104 DATA SHEET 104 Material Properties," 2015.
- [31] TA Instruments - Waters LLC, "DMA 2980 operator's manual," no. March, 2002.

- [32] C. Impact, “Accessories for CEAST Impact Systems.”
- [33] A. D7136, “Standard Test Method for Measuring the Damage Resistance of a Fiber-Reinforced Polymer Matrix Composite to a Drop-Weight Impact Event,” *ASTM Int. Des. D*, vol. i, no. C, pp. 1–16, 2005.
- [34] I. Manual, “Visual IMPACT.”

Appendices

Appendix A

A.1 Linear Viscoelastic Materials Constitutive Equation

- ❖ This analysis is restricted to one-dimensional isothermal deformations only.
- ❖ We make use of the Boltzmann Superposition Principle (BSP); *the effect of a compound cause is the sum of individual cause's' effect*; to develop this constitutive equation.

Consider the strain from a stress relaxation/ recovery experiment $\varepsilon(t) = \varepsilon_o \mathcal{H}(t)$ where $\mathcal{H}(t)$ is the Heaviside function for a step strain. The response is $\sigma_o = \varepsilon_o E(t)$ where $E(t)$ is the stress relaxation modulus. The strain can be written in terms of BSP as:

$$\varepsilon(t) = \varepsilon_o [\mathcal{H}(t) - \mathcal{H}(t - t_1)]$$

The resulting stress is:

$$\sigma(t) = \varepsilon_o [E(t) - E(t - t_1)]$$

This can be interpreted as follows: **The stress due to a delayed step strain $\varepsilon_o \mathcal{H}(t - t_1)$, $\varepsilon_o E(t - t_1)$ has the same form of time history as the stress $\varepsilon_o E(t)$ due to an earlier strain $\varepsilon_o \mathcal{H}(t)$ only differing due to a time delay.**

Note: This interpretation is only valid for non-aging materials i.e. mechanical properties do not change with time.

Now, Consider a deformation between $t - \tau$ to $t - \tau + \Delta\tau$. The strain history is given by:

$$\varepsilon(t) = \varepsilon(\tau)[\mathcal{H}(t - \tau) - \mathcal{H}(t - \tau + \Delta\tau)]$$

The increment in stress during this deformation is thus:

$$d\sigma(t) = \varepsilon(\tau)[E(t - \tau) - E(t - \tau + \Delta\tau)]$$

Mathematically:

$$\frac{dE(t - \tau)}{d\tau} = \lim_{\Delta\tau \rightarrow 0} \frac{E(t - \tau + \Delta\tau) - E(t - \tau)}{\Delta\tau}$$

Therefore, the stress increment can be re-written as:

$$d\sigma(t) = -\varepsilon(\tau) \frac{dE(t - \tau)}{d\tau} d\tau$$

This equation decomposes the entire strain history into individual pulses and the stress at a time t is the summation of each pulse's effect. By causality, only prior and up to current strains are included such that:

$$\sigma(t) = - \int_{-\infty}^t \varepsilon(\tau) \frac{dE(t - \tau)}{d\tau} d\tau$$

For an initial causal non-zero strain:

$$\Rightarrow \sigma(t) = - \int_0^t \varepsilon(\tau) \frac{dE(t - \tau)}{d\tau} d\tau + E(0) \cdot \varepsilon(t)$$

Using integration by parts, we solve as follows:

$$u = -\varepsilon(\tau), du = -\frac{d\varepsilon(\tau)}{d\tau}; dv = \frac{dE(t-\tau)}{d\tau}, v = E(t-\tau)$$

$$\therefore \sigma(t) = -\varepsilon(\tau) \cdot E(t-\tau)|_0^t - \int_0^t E(t-\tau)(-)\frac{d\varepsilon(\tau)}{d\tau} d\tau + E(0)\varepsilon(t)$$

Therefore, the stress response of a non-aging linear viscoelastic material under isothermal one-dimensional deformation is given by:

$$\sigma(t) = \int_0^t E(t-\tau) \cdot \frac{d\varepsilon(\tau)}{d\tau} d\tau$$

Where $E(t-\tau)$ is the modulus of the material. Consequently, the strain response is given by:

$$\varepsilon(t) = \int_0^t J(t-\tau) \cdot \frac{d\sigma(\tau)}{d\tau} d\tau$$

Response to Sinusoidal Loading

For a input sinusoidal strain of $\varepsilon(t) = \varepsilon_o \sin(\omega t)$, the resulting stress is:

$$\sigma(t) = \int_0^\infty E(t-\tau) \cdot \dot{\varepsilon}(\tau) d\tau = \int_0^\infty E(t-\tau) \cdot \varepsilon_o \omega \cos(\omega \tau) d\tau$$

We introduce a variable change $s = t - \tau$:

$$\sigma(t) = \int_0^\infty \varepsilon_o \omega \cdot E(s) \cos[\omega(t-s)] ds$$

Notice that:

$$\cos[\omega(t-s)] \equiv \operatorname{Re}\{e^{-i \omega(t-s)}\}$$

Therefore:

$$\sigma(t) = \varepsilon_o \omega \int_0^\infty E(s) \cdot \mathcal{Re}\{e^{-i\omega(t-s)}\} ds = \varepsilon_o \omega \int_0^\infty \cdot \mathcal{Re}\{E(s) \cdot e^{-i(t-s)}\} ds$$

$$\sigma(t) = \varepsilon_o \omega \cdot \mathcal{Re} \left[e^{-i\omega t} \cdot (-) \int_0^\infty E(s) \cdot e^{-i\omega s} ds \right]$$

The complex modulus is defined as:

$$E^* = i\omega \int_0^\infty E(s) \cdot e^{-i\omega s} ds \equiv E' + i \cdot E''$$

The stress equation is thus written as:

$$\sigma(t) = \varepsilon_o \omega \cdot \mathcal{Re} \left[e^{-i\omega t} \cdot -\frac{E^*}{i\omega} \right]$$

$$\sigma(t) = \varepsilon_o \omega \cdot \mathcal{Re} [[\cos(\omega t) + i \cdot \sin(\omega t)] \cdot [E'' - i \cdot E']]$$

$$\sigma(t) = E'' \cdot \varepsilon_o \cos(\omega t) + E' \cdot \varepsilon_o \sin(\omega t)$$

Considering the initial strain $\varepsilon(t) = \varepsilon_o \sin(\omega t)$:

$$\sigma(t) = E' \cdot \varepsilon(t) + \frac{E''}{\omega} \cdot \dot{\varepsilon}(t)$$

Considering the fundamental definition of viscoelastic stress based on the Kelvin-Voight model given

by $\sigma(t) = E' \cdot \varepsilon(t) + \eta \cdot \dot{\varepsilon}(t)$, the following relationship is defined such that $\eta \equiv \frac{E''}{\omega}$.

A.2 Stress relaxation Modulus Fourier Transform

A.2.1 Maxwell-Wiechert Fluid

$$M(t) = E e^{-\frac{t}{\tau_r}}$$

$$M^*(j\omega) = j\omega \left[\int_0^\infty E e^{-\frac{t}{\tau_r}} e^{-j\omega t} dt \right]$$

$$M^*(j\omega) = j\omega E \int_0^\infty e^{-\frac{1+j\omega\tau_r}{\tau_r} t} dt$$

$$M^*(j\omega) = j\omega E \frac{\tau_r}{1+j\omega\tau_r} e^{-\frac{1+j\omega\tau_r}{\tau_r} t} \Big|_0^\infty$$

$$M^*(j\omega) = E \frac{j\omega\tau_r}{1+j\omega\tau_r}$$

$$M^*(j\omega) = E \cdot \frac{(\omega\tau_r)^2}{1 + (\omega\tau_r)^2} + j \cdot E \cdot \frac{\omega\tau_r}{1 + (\omega\tau_r)^2}$$

A.2.2 Kelvin-Voigt Solid

$$M(t) = E \cdot H(t) + \eta \cdot \delta(t)$$

$$M^*(j\omega) = j\omega \left[\int_0^\infty [E \cdot H(t) + \eta \cdot \delta(t)] e^{-j\omega t} dt \right]$$

$$M^*(j\omega) = j\omega \left[\int_0^\infty E \cdot H(t) e^{-j\omega t} dt + \int_0^\infty \eta \cdot \delta(t) e^{-j\omega t} dt \right]$$

$$M^*(j\omega) = E \cdot e^{-j\omega t} \Big|_0^\infty + j\omega\eta \int_0^\infty \delta(t) e^{-j\omega t} dt$$

$$M^*(j\omega) = E + j \cdot \eta \cdot \omega$$

A.2.3 Standard Linear Solid

$$M(t) = \frac{q_o}{p_o} + \left[\frac{q_1}{p_1} - \frac{q_o}{p_o} \right] e^{-\frac{t}{\tau}}$$

$$M^*(j\omega) = j\omega \left[\int_0^\infty \left(\frac{q_o}{p_o} + \left[\frac{q_1}{p_1} - \frac{q_o}{p_o} \right] e^{-\frac{t}{\tau}} \right) e^{-j\omega t} dt \right]$$

$$M^*(j\omega) = j\omega \left[\int_0^\infty \frac{q_o}{p_o} \cdot e^{-j\omega t} dt + \int_0^\infty \left[\frac{q_1}{p_1} - \frac{q_o}{p_o} \right] e^{-\frac{1+j\omega}{\tau} t} dt \right]$$

$$M^*(j\omega) = \frac{q_o}{p_o} e^{-j\omega t} \Big|_0^\infty + \left[\frac{q_1}{p_1} - \frac{q_o}{p_o} \right] \cdot \frac{j\omega\tau}{1 + j\omega\tau} e^{-\frac{1+j\omega}{\tau} t} \Big|_0^\infty$$

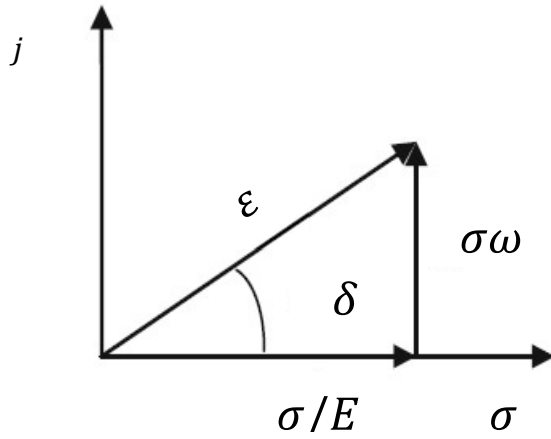
$$M^*(j\omega) = \frac{q_o}{p_o} + \left[\frac{q_1}{p_1} - \frac{q_o}{p_o} \right] \cdot \frac{j\omega\tau + (\omega\tau)^2}{1 + (\omega\tau)^2}$$

$$M^*(j\omega) = \frac{q_o}{p_o} + \left[\frac{q_1}{p_1} - \frac{q_o}{p_o} \right] \cdot \frac{(\omega\tau)^2}{1 + (\omega\tau)^2} + j \cdot \left[\frac{q_1}{p_1} - \frac{q_o}{p_o} \right] \cdot \frac{\omega\tau}{1 + (\omega\tau)^2}$$

$$p_o \equiv E_o + E_k; \quad p_1 \equiv \eta_k; \quad q_o \equiv E_o E_k; \quad q_1 \equiv E_o \eta_k; \quad \tau = \frac{p_1}{p_o}$$

A.3 Experimental Loss and Storage Moduli

A.3.1 Maxwell Model



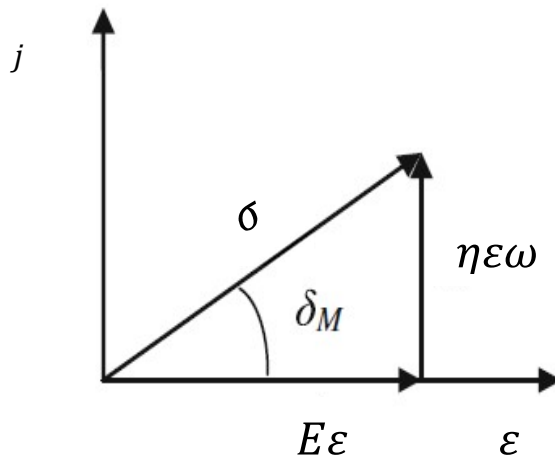
$$\varepsilon \cdot \cos \delta = \frac{\sigma}{E} \Rightarrow \frac{X}{L_o} \cos \delta = \frac{F}{A} \frac{1}{E}$$

$$\therefore E = \frac{F L_o}{A X} \frac{1}{\cos \delta} \equiv E'$$

$$\varepsilon \cdot \sin \delta = \frac{\sigma \omega}{\eta} \Rightarrow \frac{X}{L_o} \sin \delta = \frac{F}{A} \frac{\omega}{\eta}$$

$$\therefore \eta \omega = \frac{F L_o}{A X} \omega^2 \frac{1}{\sin \delta} \equiv E''$$

A.3.2 Kelvin Model



$$E\varepsilon = \sigma \cdot \cos \delta \Rightarrow \frac{F}{A} \cos \delta = E \frac{X}{L_o}$$

$$\therefore E = \frac{F L_o}{A X} \cos \delta \equiv E'$$

$$\eta\varepsilon\omega = \sigma \cdot \sin \delta \Rightarrow \frac{F}{A} \sin \delta = \eta\omega \frac{X}{L_o}$$

$$\therefore \eta\omega = \frac{F L_o}{A X} \sin \delta \equiv E''$$

Appendix B

B.1 Damping Ratio change with Frequency

$$\zeta = \frac{A E' \tan \delta}{L} \frac{1}{\omega} \frac{1}{2m \sqrt{\frac{k}{m}}} = \frac{\sqrt{A}}{2\omega \sqrt{Lm}} \sqrt{E'} \tan \delta$$

If the causing frequency matches the system natural frequency, the damping ratio is:

$$\zeta = \frac{A E' \tan \delta}{L} \frac{1}{\omega_n} \frac{1}{2m \omega_n} = \frac{A E' \tan \delta}{L} \frac{1}{\omega_n^2} \frac{1}{2m} = \frac{A E' \tan \delta}{L} \frac{1}{\frac{k}{m}} \frac{1}{2m}$$

Substituting stiffness and simplifying yields:

$$\zeta = \frac{A E' \tan \delta}{L} \frac{L}{A E'} \frac{1}{2m} = \frac{\tan \delta}{2}$$

B.2 Predicted Peak Strain Calculation

$$m \cdot a_{max} = F = K \cdot x$$

Divide both sides of the equation by thickness to obtain strain:

$$m \cdot \frac{a_{max}}{L} = \frac{F}{L} = k \cdot \frac{x}{L}$$

$$m \cdot \frac{a_{max}}{k \cdot L} = \frac{x}{L}$$

Using the definition $k = E \cdot \frac{A}{L}$:

$$\frac{x}{L} = m \cdot \frac{a_{max}}{A \cdot E}$$

B.3 Viscous Model Simulated Response

For a second order viscous model with a spring and dashpot, once contact is made by the dropping mass, the system is a simple mass spring damper system with initial velocity v_0 , and initial displacement $x_0 = 0$. The equation of motion is thus:

$$m\ddot{x} + c\dot{x} + kx = 0$$

Or can be expressed in terms of the natural frequency as:

$$\ddot{x} + 2\zeta\omega_n\dot{x} + \omega_n^2x = 0$$

Where $\omega_n = \sqrt{\frac{k}{m}}$, and $2\zeta\omega_n = \frac{c}{m}$

The solution of this differential equation is given by:

$$x = \frac{v_0}{\omega_d} e^{-\zeta\omega_n t} \sin(\omega_d t)$$

The velocity and acceleration of the mass from the point of contact to maximum deformation are given by:

$$v = v_0 e^{-\zeta\omega_n t} \left(-\frac{\zeta\omega_n}{\omega_d} \sin(\omega_d t) + \cos(\omega_d t) \right)$$

$$a = v_0 e^{-\zeta\omega_n t} \left(\frac{\zeta^2\omega_n^2}{\omega_d} \sin(\omega_d t) - 2\zeta\omega_n \cos(\omega_d t) - \omega_d \sin(\omega_d t) \right)$$

The time response plots for the displacement, velocity and acceleration for $m=1\text{kg}$, $k=100\text{kN/m}$, $\zeta=0.2$, and an initial velocity at impact of $v_0=4.4\text{m/s}$ are given in the figure below with the positive frame of reference defined in the same direction as gravity:

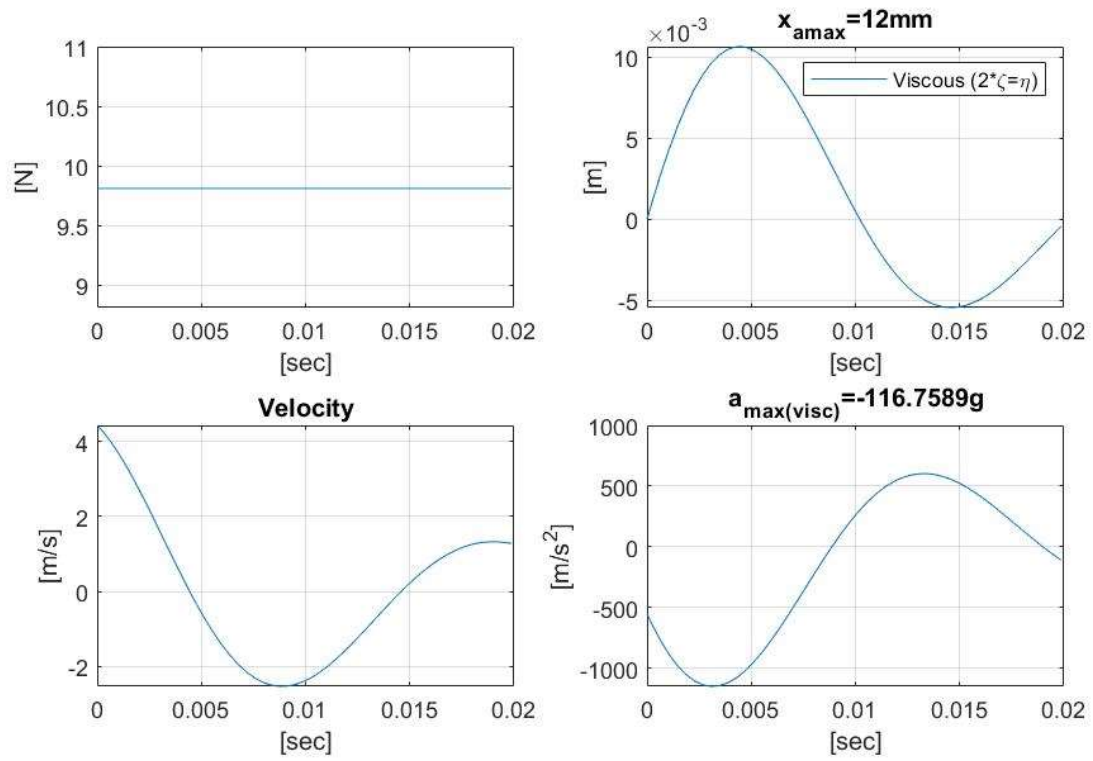


Figure 6-1: Viscous Impact Model Response Prediction

Appendix C

C.1 Data Tables

Table C-1: Sorbothane Sample Raw Material Data

f [Hz]	F_A [N]	X_A [μm]	k [N/m]	$\tan \delta$	E' [Pa]	m [kg]	$\frac{A}{Lm}$ [$\frac{m}{kg}$]	$\left(\frac{a}{v}\right)^2$ [$\frac{1}{s^2}$]
10.0	0.0986604	18.10661	5447.939	0.520744	367112.3761	1.86590	0.00961	1543.55
11.8	0.1010378	18.05217	5596.387	0.550576	372464.2545	1.37658	0.01299	2029.53
13.6	0.1060419	17.96567	5901.827	0.576872	388337.4361	1.09286	0.01633	2567.21
15.5	0.1158923	17.87515	6483.096	0.579435	426027.8882	0.92422	0.01929	3322.10
17.2	0.1270024	17.81147	7130.410	0.571839	470092.2936	0.82550	0.02159	4148.77
19.2	0.1443621	17.81632	8102.739	0.565952	535440.8576	0.75281	0.02373	5226.78
21.0	0.1576540	17.80720	8853.521	0.559435	586644.4265	0.68760	0.02603	6327.30
22.8	0.1688511	17.79114	9490.710	0.557358	629441.936	0.62530	0.02867	7485.49
24.6	0.1801312	17.78482	10128.832	0.556061	672175.7898	0.57325	0.03130	8733.52
26.5	0.1924714	17.80583	10810.167	0.555099	717743.1198	0.52723	0.03406	10151.35
28.4	0.2035810	17.79815	11438.123	0.557335	758770.9051	0.48571	0.03699	11608.91
30.2	0.2148121	17.80569	12063.763	0.557004	800419.1353	0.45303	0.03967	13134.60
32.0	0.2263715	17.83703	12690.793	0.557656	841831.8815	0.42447	0.04234	14728.13
33.8	0.2357263	17.86324	13195.387	0.562594	873503.9686	0.39559	0.04543	16279.56
35.6	0.2463337	17.90407	13759.087	0.564755	909975.9511	0.37183	0.04831	17987.41
37.6	0.2561486	17.93985	14280.057	0.565254	944266.3067	0.34595	0.05190	20045.81
39.4	0.2652683	17.97043	14763.643	0.567926	975154.4876	0.32573	0.05508	21901.71
41.2	0.2739180	18.00214	15217.550	0.571401	1003659.272	0.30705	0.05839	23794.98
43.0	0.2827805	18.02393	15690.900	0.575135	1033220.122	0.29065	0.06164	25742.62
44.8	0.2901625	18.02742	16096.900	0.583799	1056012.834	0.27469	0.06518	27507.47
46.6	0.3003905	18.04410	16648.860	0.589074	1089747.302	0.26258	0.06814	29483.49
48.6	0.3124074	18.05674	17302.600	0.582910	1135644.817	0.25090	0.07126	32423.12
50.5	0.3229680	18.06132	17882.833	0.578693	1175824.7	0.24017	0.07438	35275.16
52.0	0.3316307	18.06146	18361.853	0.577569	1207902.282	0.23258	0.07676	37478.79
54.0	0.3399529	18.05830	18825.747	0.578841	1237747.497	0.22112	0.08071	40323.84
55.0	0.3460481	18.04975	19172.310	0.580064	1259872.565	0.21707	0.08218	41738.37
57.0	0.3529855	18.05219	19553.990	0.581702	1284048.492	0.20613	0.08651	44696.69
59.5	0.3592992	18.04908	19907.133	0.585748	1304934.173	0.19259	0.09257	48352.99
61.5	0.3654092	18.04885	20245.773	0.589047	1325228.463	0.18333	0.09723	51357.53
63.5	0.3711672	18.04614	20567.853	0.592475	1344314.282	0.17470	0.10201	54423.53
65.0	0.3767278	18.04627	20875.850	0.595180	1362817.526	0.16923	0.10528	56756.55
66.0	0.3814044	18.04163	21140.410	0.595759	1379740.048	0.16622	0.10717	58456.53

Table C-1: Sorbothane Sample Raw Material Data (continued)

f [Hz]	F_A [N]	X_A [μm]	k [N/m]	$\tan \delta$	E' [Pa]	m [kg]	$\frac{A}{Lm} [\frac{m}{kg}]$	$(\frac{a}{v})^2 [\frac{1}{s^2}]$
68.0	0.3866960	18.04116	21434.207	0.598151	1397438.929	0.15876	0.11219	61799.15
70.5	0.3929848	18.04197	21781.840	0.601051	1418279.582	0.15010	0.11864	66102.62
72.5	0.3989062	18.04248	22109.357	0.600114	1440200.434	0.14406	0.12360	70018.42
74.5	0.4040081	18.04085	22394.150	0.600762	1458343.753	0.13819	0.12884	73853.09
76.0	0.4082566	18.03863	22632.413	0.602399	1472801.792	0.13420	0.13266	76644.33
77.0	0.4114183	18.03740	22809.213	0.604008	1483254.46	0.13176	0.13512	78462.51
79.0	0.4151094	18.03482	23017.133	0.609488	1493145.25	0.12631	0.14094	81850.14
81.5	0.4195121	18.03465	23261.493	0.609701	1508857.614	0.11994	0.14842	87081.84
83.5	0.4208873	18.03382	23338.777	0.613914	1511026.25	0.11465	0.15528	90798.32
85.5	0.4208161	18.03045	23339.197	0.622824	1505048.305	0.10935	0.16280	93912.09
87.0	0.4205737	18.02913	23327.467	0.637247	1494546.318	0.10556	0.16865	95343.82
88.0	0.4220457	18.03058	23407.217	0.647134	1492930.836	0.10352	0.17196	96474.18
90.0	0.4285178	18.03457	23760.923	0.651098	1512750.327	0.10047	0.17718	100528.39
92.5	0.4300024	18.03112	23847.827	0.656361	1514614.954	0.09546	0.18647	105788.35
94.5	0.4270990	18.02795	23690.917	0.678556	1489326.711	0.09086	0.19594	110295.37
96.5	0.4372614	18.03637	24243.320	0.698873	1509680.119	0.08916	0.19966	121328.38
98.0	0.4516607	18.04031	25036.203	0.682550	1570987.9	0.08928	0.19938	119242.12
100.0	0.4643570	18.04243	25736.927	0.676598	1619471.379	0.08815	0.20196	123240.01

Table C-2: Neoprene Sample Raw Material Data

f [Hz]	F_A [N]	X_A [μm]	k [N/m]	$\tan \delta$	E' [Pa]	m [kg]	$\frac{A}{Lm} [\frac{m}{kg}]$	$(\frac{a}{v})^2 [\frac{1}{s^2}]$
10.0	0.243279	18.01495	13502.11	0.2053	951344.5	4.67562	0.00412	2803.06
11.8	0.259327	18.02887	14384.12	0.2211	1010718.5	3.57731	0.00543	3797.59
13.6	0.272915	18.01472	15143.44	0.2394	1059429.7	2.83520	0.00679	4878.97
15.5	0.289582	17.96734	16113.79	0.2272	1130257.4	2.32259	0.00832	6477.09
17.2	0.292470	18.00791	16243.71	0.2344	1138172.0	1.90137	0.01022	7879.33
19.2	0.289229	18.08548	15992.67	0.3011	1102403.3	1.50230	0.01287	8743.20
21.0	0.304690	18.08698	16845.00	0.3528	1142665.9	1.32273	0.01439	9436.45
22.8	0.350708	18.02456	19456.90	0.3455	1322712.8	1.29611	0.01467	11270.50
24.6	0.399357	17.97404	22218.21	0.3045	1528717.9	1.27138	0.01495	14169.75
26.5	0.441230	17.93540	24600.35	0.2580	1713249.5	1.21307	0.01568	17911.03
28.4	0.464911	17.91204	25954.68	0.2258	1820977.5	1.11434	0.01707	21800.49
30.2	0.481373	17.93263	26843.11	0.2103	1889413.2	1.01919	0.01867	25339.62
32.0	0.493764	17.97807	27464.55	0.2025	1936166.5	0.92877	0.02049	28847.91
33.8	0.502531	17.98850	27935.92	0.1984	1970953.8	0.84677	0.02247	32417.20
35.6	0.510397	18.00757	28343.09	0.1974	2000043.9	0.77444	0.02456	36022.37

Table C-2: Neoprene Sample Raw Material Data (continued)

f [Hz]	F_A [N]	X_A [μm]	k [N/m]	$\tan \delta$	E' [Pa]	m [kg]	$\frac{A}{Lm}$ [$\frac{m}{kg}$]	$\left(\frac{a}{v}\right)^2$ [$\frac{1}{s^2}$]
37.6	0.517287	18.01535	28713.25	0.1962	2026645.9	0.70331	0.02705	40272.69
39.4	0.522369	18.02570	28978.77	0.1961	2045421.1	0.64644	0.02943	44227.49
41.2	0.526783	18.03445	29209.28	0.1973	2061218.7	0.59589	0.03192	48257.88
43.0	0.531890	18.04462	29476.04	0.1992	2079266.0	0.55204	0.03445	52386.64
44.8	0.536116	18.04431	29710.58	0.2016	2094832.6	0.51262	0.03710	56622.96
46.6	0.542449	18.03370	30079.38	0.2050	2119443.2	0.47966	0.03965	60901.39
48.6	0.549660	18.02016	30502.31	0.2033	2149997.6	0.44720	0.04253	66448.34
50.5	0.555862	18.03950	30813.23	0.2021	2172400.6	0.41840	0.04545	71893.51
52.0	0.560249	18.05819	31024.99	0.2007	2187923.9	0.39732	0.04786	76417.66
54.0	0.564026	18.09885	31163.76	0.2006	2197745.4	0.37008	0.05138	82421.46
55.0	0.565736	18.08922	31274.84	0.2009	2205449.4	0.35802	0.05311	85456.20
57.0	0.567235	18.09207	31352.75	0.2024	2210297.6	0.33417	0.05690	91540.04
59.5	0.568331	18.09304	31411.79	0.2045	2213544.8	0.30725	0.06188	99375.80
61.5	0.569801	18.09594	31487.80	0.2059	2218301.2	0.28829	0.06595	105914.07
63.5	0.569790	18.08833	31500.41	0.2072	2218592.9	0.27052	0.07028	112643.35
65.0	0.569601	18.08341	31498.48	0.2095	2217468.7	0.25817	0.07365	117562.01
66.0	0.569739	18.08265	31507.45	0.2113	2217296.1	0.25047	0.07591	120820.07
68.0	0.568679	18.07902	31455.03	0.2155	2211709.2	0.23556	0.08072	127294.64
70.5	0.569171	18.08346	31474.69	0.2180	2211941.5	0.21929	0.08670	136217.46
72.5	0.566242	18.07807	31322.08	0.2197	2200411.0	0.20635	0.09214	143608.05
74.5	0.561181	18.07267	31051.38	0.2241	2179364.8	0.19373	0.09814	150454.24
76.0	0.555834	18.06913	30761.53	0.2293	2156607.6	0.18442	0.10310	155126.91
77.0	0.550463	18.06868	30465.02	0.2341	2133600.4	0.17793	0.10686	157890.58
79.0	0.539636	18.06123	29878.18	0.2470	2086364.9	0.16578	0.11469	162374.20
81.5	0.528224	18.06422	29241.59	0.2710	2030053.8	0.15245	0.12471	165435.76
83.5	0.525809	18.08208	29079.00	0.2808	2013656.2	0.14443	0.13162	170561.46
85.5	0.529043	18.08850	29247.46	0.2788	2026360.6	0.13855	0.13721	179486.65
87.0	0.531769	18.08876	29397.74	0.2783	2037030.9	0.13450	0.14135	186005.06
88.0	0.534162	18.08984	29528.25	0.2790	2045707.1	0.13204	0.14399	190057.53
90.0	0.539678	18.09253	29828.68	0.2821	2064874.0	0.12752	0.14911	197664.53
92.5	0.542833	18.09310	30002.12	0.2845	2075595.7	0.12142	0.15661	207876.97
94.5	0.539325	18.08709	29818.11	0.2956	2056761.9	0.11563	0.16448	212555.93
96.5	0.507765	18.09552	28061.12	0.3905	1883827.5	0.10435	0.18527	188232.74
98.0	0.503008	17.89693	28105.50	0.4238	1862653.1	0.10134	0.18979	180977.09
100.0	0.470812	18.09000	26026.13	0.5231	1657010.2	0.09013	0.21092	155369.30

Table C-3: Rubber Sample Raw Material Data

f [Hz]	F_A [N]	X_A [μm]	k [N/m]	$\tan \delta$	E' [Pa]	m [kg]	$\frac{A}{Lm} [\frac{m}{kg}]$	$(\frac{a}{v})^2 [\frac{1}{s^2}]$
10.0	1.92481	17.77611	108276.30	0.271403	6846192.876	38.45200	0.000558	2488.782987
11.8	1.94798	17.74576	109767.97	0.277639	6929573.571	27.99607	0.000766	3425.973488
13.6	1.98699	17.73500	112035.33	0.283874	7061213.816	21.51110	0.000996	4499.049089
15.5	2.03120	17.73383	114536.97	0.290275	7206647.968	16.93042	0.001266	5775.369986
17.2	2.07243	17.72697	116906.77	0.296116	7344184.145	14.03357	0.001527	7035.262689
19.2	2.11870	17.72345	119541.13	0.302714	7496077.599	11.51597	0.001860	8659.831618
21.0	2.16616	17.72954	122177.77	0.308465	7649101.604	9.83873	0.002177	10249.42669
22.8	2.20614	17.72668	124452.77	0.315077	7776913.152	8.50199	0.002519	11933.62302
24.6	2.24692	17.72668	126753.17	0.321024	7907067.13	7.43831	0.002879	13738.50491
26.5	2.28907	17.73072	129101.77	0.327390	8038545.34	6.52869	0.003280	15753.40143
28.4	2.32559	17.72984	131167.47	0.334342	8150245.446	5.77531	0.003708	17858.20573
30.2	2.36178	17.73033	133205.37	0.340540	8261340.14	5.18673	0.004129	19958.83647
32.0	2.40286	17.73485	135488.23	0.346556	8387370.914	4.69880	0.004557	22155.4154
33.8	2.42984	17.73534	137005.10	0.354001	8461614.424	4.25882	0.005028	24371.26376
35.6	2.46466	17.73451	138974.63	0.361028	8564154.352	3.89422	0.005498	26677.09556
37.6	2.50093	17.73386	141025.13	0.368737	8668966.368	3.54247	0.006044	29324.15214
39.4	2.53764	17.73345	143098.43	0.375731	8776329.762	3.27362	0.006540	31770.98202
41.2	2.57483	17.73353	145194.83	0.382801	8884062.656	3.03768	0.007048	34272.21292
43.0	2.61556	17.73769	147457.47	0.389241	9003006.383	2.83214	0.007559	36872.83732
44.8	2.63568	17.73958	148575.97	0.395296	9052679.114	2.62892	0.008143	39560.06628
46.6	2.65336	17.74322	149542.10	0.406001	9077960.108	2.44555	0.008754	41926.56506
48.6	2.68038	17.74130	151081.27	0.415201	9141835.313	2.27156	0.009425	44796.84789
50.5	2.69841	17.74789	152041.20	0.423706	9172070.669	2.11721	0.010112	47575.36057
52.0	2.71372	17.75395	152852.00	0.431969	9193521.294	2.00747	0.010665	49638.51699
54.0	2.72099	17.76079	153202.20	0.445132	9170138.354	1.86579	0.011475	52173.35599
55.0	2.72230	17.76471	153242.20	0.454442	9140681.926	1.79903	0.011901	53147.85525
57.0	2.72608	17.76437	153458.23	0.469849	9100049.892	1.67736	0.012764	55388.35186
59.5	2.73698	17.76303	154082.60	0.489784	9066270.893	1.54563	0.013850	58044.3425
61.5	2.76506	17.75225	155757.60	0.505311	9108267.038	1.46246	0.014636	60159.57317
63.5	2.82374	17.73892	159183.00	0.512373	9281839.362	1.40196	0.015267	63260.89583
65.0	2.89179	17.73287	163074.73	0.512692	9507485.255	1.37071	0.015614	66244.79251
66.0	2.95128	17.73290	166429.57	0.511566	9707518.476	1.35684	0.015774	68448.86829
68.0	3.03982	17.72213	171526.50	0.503572	10037141.59	1.31734	0.016247	73801.09659
70.5	3.09736	17.72236	174771.27	0.508272	10207669.03	1.24876	0.017139	78605.24081
72.5	3.16166	17.72214	178401.33	0.513811	10396320.41	1.20533	0.017756	82235.41472
74.5	3.24350	17.71528	183090.10	0.512423	10675592.01	1.17149	0.018269	87069.75219
76.0	3.31214	17.72247	186889.30	0.512716	10895807.24	1.14906	0.018625	90560.05468

Table C-3: Rubber Sample Raw Material Data (continued)

f [Hz]	F_A [N]	X_A [μm]	k [N/m]	$\tan \delta$	E' [Pa]	m [kg]	$\frac{A}{Lm} [\frac{m}{kg}]$	$(\frac{a}{v})^2 [\frac{1}{s^2}]$
77.0	3.36402	17.73008	189735.27	0.514803	11052344.83	1.13645	0.018832	92582.79196
79.0	3.43271	17.72888	193622.20	0.515751	11274396.43	1.10176	0.019425	97275.2368
81.5	3.51378	17.71560	198343.43	0.514081	11557157.1	1.06044	0.020182	103865.6384
83.5	3.58753	17.71373	202528.40	0.513817	11802280.57	1.03157	0.020747	109081.2505
85.5	3.65819	17.71413	206512.47	0.514090	12033118.09	1.00323	0.021334	114308.0383
87.0	3.72202	17.72333	210006.60	0.515300	12230694.04	0.98533	0.021722	118075.7525
88.0	3.77205	17.73078	212740.30	0.517485	12378859.41	0.97560	0.021939	120293.8999
90.0	3.82888	17.73161	215935.40	0.519531	12554299.05	0.94673	0.022608	125323.8108
92.5	3.88068	17.72593	218926.97	0.521465	12718166.66	0.90866	0.023556	131886.3382
94.5	3.92183	17.72867	221214.27	0.524290	12836050.7	0.87970	0.024332	136901.2504
96.5	3.98057	17.72499	224574.17	0.531822	12990703.58	0.85643	0.024994	140691.5617
98.0	4.04624	17.72922	228224.03	0.532056	13200571.65	0.84391	0.025364	145033.4826
100.0	4.10439	17.73302	231453.87	0.533559	13379084.12	0.82196	0.026041	150575.809

Table C-4: Santoprene Sample Raw Material Data

f [Hz]	F_A [N]	X_A [μm]	k [N/m]	$\tan \delta$	E' [Pa]	m [kg]	$\frac{A}{Lm} [\frac{m}{kg}]$	$(\frac{a}{v})^2 [\frac{1}{s^2}]$
10.0	3.0619	19.617	156062.6	0.14228	11651306.6	52.5956	0.00034	3127.364
11.8	3.1551	19.588	161045.0	0.14373	12021050.6	38.9793	0.00046	4343.765
13.6	3.2559	19.587	166204.7	0.14451	12404963.5	30.2842	0.00059	5762.354
15.5	3.3489	19.605	170806.6	0.14563	12746481.3	23.9603	0.00074	7470.630
17.2	3.4331	19.596	175178.4	0.14677	13070647.2	19.9560	0.00089	9181.322
19.2	3.5185	19.598	179526.0	0.14807	13392521.7	16.4125	0.00108	11415.251
21.0	3.5947	19.617	183237.3	0.14919	13667131.9	14.0032	0.00126	13629.749
22.8	3.6606	19.604	186724.2	0.15063	13924225.5	12.1055	0.00146	16026.962
24.6	3.7332	19.606	190407.6	0.15165	14196667.8	10.6039	0.00167	18624.652
26.5	3.8007	19.618	193734.4	0.15272	14442345.2	9.2975	0.00190	21573.098
28.4	3.8596	19.612	196801.8	0.15398	14668162.2	8.2232	0.00215	24724.347
30.2	3.9198	19.614	199851.7	0.15503	14892979.5	7.3849	0.00239	27907.584
32.0	3.9811	19.631	202797.9	0.15656	15108850.4	6.6744	0.00265	31250.951
33.8	4.0274	19.621	205269.0	0.15777	15290041.4	6.0554	0.00292	34793.135
35.6	4.0783	19.622	207853.0	0.15919	15479006.7	5.5272	0.00320	38503.278
37.6	4.1281	19.623	210377.6	0.16098	15662523.7	5.0150	0.00353	42819.414
39.4	4.1720	19.626	212585.8	0.16292	15821953.1	4.6152	0.00383	46860.120
41.2	4.2133	19.628	214670.6	0.16551	15970188.9	4.2622	0.00415	51011.190
43.0	4.2588	19.640	216843.5	0.16863	16123056.0	3.9524	0.00448	55268.432
44.8	4.3012	19.630	219118.2	0.17022	16287526.5	3.6794	0.00481	59829.011

Table C-4: Santoprene Sample Raw Material Data (continued)

f [Hz]	F_A [N]	X_A [μm]	k [N/m]	$\tan \delta$	E' [Pa]	m [kg]	$\frac{A}{Lm} [\frac{m}{kg}]$	$(\frac{a}{v})^2 [\frac{1}{s^2}]$
46.6	4.3480	19.629	221510.8	0.17212	16459853.7	3.4377	0.00515	64520.403
48.6	4.3959	19.629	223962.6	0.17321	16638863.6	3.1956	0.00555	70045.560
50.5	4.4502	19.635	226651.8	0.17332	16838399.8	2.9952	0.00592	75613.973
52.0	4.4923	19.642	228713.3	0.17224	16995267.9	2.8506	0.00623	80318.534
54.0	4.5088	19.648	229486.3	0.17329	17050497.4	2.6523	0.00670	86456.064
55.0	4.5207	19.652	230039.9	0.17463	17088131.1	2.5629	0.00694	89478.395
57.0	4.5183	19.658	229849.4	0.17933	17060715.1	2.3842	0.00746	95320.273
59.5	4.4924	19.662	228483.2	0.19012	16927543.0	2.1751	0.00818	101926.108
61.5	4.4758	19.661	227653.2	0.20073	16832908.1	2.0285	0.00877	106882.715
63.5	4.4654	19.661	227118.2	0.21602	16742563.6	1.8983	0.00936	110903.328
65.0	4.4929	19.657	228554.3	0.22560	16813618.3	1.8231	0.00973	114234.047
66.0	4.5238	19.653	230177.1	0.23015	16914869.8	1.7808	0.00995	116822.401
68.0	4.5858	19.646	233416.9	0.23192	17144849.5	1.7012	0.01041	123624.980
70.5	4.6887	19.636	238781.6	0.23319	17529289.5	1.6191	0.01093	132626.659
72.5	4.7430	19.636	241549.8	0.23506	17722339.1	1.5487	0.01143	139818.863
74.5	4.8505	19.631	247082.2	0.23443	18129415.5	1.5003	0.01181	147822.856
76.0	4.9571	19.634	252480.7	0.23078	18537581.4	1.4732	0.01203	154877.438
77.0	5.0402	19.636	256680.3	0.22642	18862971.1	1.4590	0.01216	160227.036
79.0	5.1527	19.633	262465.7	0.21446	19338893.6	1.4173	0.01255	172242.220
81.5	5.2372	19.628	266846.7	0.20342	19709550.1	1.3539	0.01317	186870.788
83.5	5.2944	19.632	269706.4	0.19675	19949051.8	1.3037	0.01370	198445.721
85.5	5.3324	19.637	271568.9	0.19268	20104129.7	1.2520	0.01428	209543.085
87.0	5.3586	19.648	272749.1	0.19102	20198563.5	1.2144	0.01473	217583.420
88.0	5.3805	19.652	273802.3	0.19037	20279592.1	1.1916	0.01502	222864.348
90.0	5.3956	19.655	274531.5	0.19060	20333241.2	1.1422	0.01567	233015.499
92.5	5.4043	19.651	275024.8	0.19079	20369683.4	1.0833	0.01653	246054.732
94.5	5.4101	19.652	275305.0	0.19174	20387231.5	1.0390	0.01724	256378.205
96.5	5.4228	19.651	275963.1	0.19459	20425377.6	0.9987	0.01794	266008.978
98.0	5.4493	19.651	277314.5	0.19545	20522439.4	0.9731	0.01842	273927.716
100.0	5.4775	19.650	278760.2	0.19692	20623997.8	0.9395	0.01908	284482.014

C.2 Sample Calculations

Table 5-1 to Table 5-3: Predicted Peak Acceleration

The maximum acceleration equation from the impact absorption analysis in Chapter 3 is recalled below. Using the drop tower parameters of mass, material thickness and effective area as well as the dynamic material properties from the DMA, we can predict the performance of a material for a given input velocity.

$$\left(\frac{a_{max}}{v_o}\right)^2 = \left(\frac{A}{Lm}\right) \left(E' e^{-\frac{2 \tan \delta \arctan\left(\frac{\sqrt{4-\tan^2(\tan \delta^2-1)}}{\tan \delta(\tan \delta^2-3)}\right)}{\sqrt{4-\tan^2}}}\right)$$

Let us consider an $\frac{A}{Lm} = 0.01 \text{ m/kg}$. At this design point, using the chart in Figure 4-7, Sorbothane has a storage modulus of $E' = 400835.98 \text{ MPa}$ and a loss factor of $\tan \delta = 0.523$. Given the drop tower impact mass is 3.337 kg and the effective impacted material area is $A = (8 \times 10^{-3})^2 \pi \text{ m}^2$ and a thickness of $L = 6.55 \times 10^{-3} \text{ m}$, we can predict the resulting acceleration from an initial velocity at impact of $v_o = 1 \frac{\text{m}}{\text{s}}$ as follows: as:

$$a_{max} = \sqrt{1 * (8 \times 10^{-3})^2 \frac{\pi}{6.55 \times 10^{-3} * 3.337} * 400835.98' e^{-\frac{2 * 0.523 \arctan\left(\frac{\sqrt{4-0.523^2}(0.523^2-1)}{0.523(0.523^2-3)}\right)}{\sqrt{4-0.523^2}}}} = 51.40 \text{ m/s}^2$$

This calculation is repeated for the rest of the values in Tables 5-1, 5-2, and 5-3.

Table 4-3, Table C-1 to C-4: Raw Material Data

Due to inconsistencies with the produced DMA data, manual calculation of material properties is required. Using the raw measured signals from the frequency sweep, we can generate all material properties. The raw signals from the DMA are the amplitude of the force, F_A , the deformation amplitude, X_A , and the loss factor, $\tan \delta$. Also given are the geometric parameters of area, A , thickness, L , and the resulting correction factor, F_e which accounts for lateral strain. This calculation uses the data from the first Sorbothane run at a frequency of 70.5 Hz. The cross sectional area and thickness of Sorbothane are $A = 1.07 \times 10^{-4} \text{ m}^2$ and $L = 6.01 \times 10^{-3} \text{ m}$ which result in a correction factor $F_e = 0.74$. The raw DMA signals at this frequency are:

$$F_A = 0.41 \text{ N}; X_A = 18.04 \mu\text{m}; \tan \delta = 0.607$$

We can determine the true stiffness k using the amplitude force and displacement and correct for lateral strain using F_e .

$$k = \frac{\left(\frac{F_A}{X_A}\right)}{F_e} = \frac{\frac{0.41}{18.04 \times 10^{-6}}}{0.74} = 22,535.08 \text{ N/m}$$

The resulting storage modulus is then:

$$E' = \frac{kL}{A} \cos \delta = \frac{22,535.08 \times 6.01 \times 10^{-3}}{1.07 \times 10^{-4}} \times \cos(\tan^{-1} 0.607) = 1.46 \text{ MPa}$$

Now we determine the mass required to convert the current frequency to the system natural frequency. This is done by converting the frequency to radians and using the natural frequency equation for a second order viscous model, the mass is:

$$m = \frac{k}{\omega_n^2} = \frac{22,535.08}{(70.5 * 2\pi)^2} = 0.16 \text{ kg}$$

With mass, thickness and area all obtained, the ratio $\frac{A}{Lm}$ is calculated as:

$$\frac{A}{Lm} = \frac{1.07 \times 10^{-4}}{6.01 \times 10^{-3} \times 0.16} = 0.1146 \text{ m/kg}$$

This calculation is repeated to obtain the values in Table 6-1 to 6-4. The formulae are summarized in Table 4-3.